Review article

Guang-Can Li, Qiang Zhang, Stefan A. Maier and Dangyuan Lei*

Plasmonic particle-on-film nanocavities: a versatile platform for plasmon-enhanced spectroscopy and photochemistry

https://doi.org/10.1515/nanoph-2018-0162
Received September 27, 2018; accepted October 13, 2018

Abstract: Metallic nanostructures with nanometer gaps support hybrid plasmonic modes with an extremely small mode volume and strong local field intensity, which constitutes an attractive plasmonic platform for exploring novel light-matter interaction phenomena at the nanoscale. Particularly, the plasmonic nanocavity formed by a metal nanoparticle closely separated from a thin metal film has received intensive attention in the nanophotonics community, largely attributed to its ease of fabrication, tunable optical properties over a wide spectral range, and the ultrastrong confinement of light at the small gap region scaled down to sub-nanometer. In this article, we review the recent exciting progress in exploring the plasmonic properties of such metal particle-on-film nanocavities (MPoFNs), as well as their fascinating applications in the area of plasmon-enhanced imaging and spectroscopies. We focus our discussion on the experimental fabrication and optical characterization of MPoFNs and the theoretical interpretation of their hybridized plasmon modes, with particular interest on the nanocavity-enhanced photoluminescence and Raman spectroscopies, as well as photocatalysis and molecular nanochemistry.

Keywords: particle-on-film nanocavities; plasmon coupling; spontaneous emission; Raman spectroscopy; photocatalysis and photochemistry.

***Corresponding author: Dangyuan Lei,** Department of Applied physics, The Hong Kong Polytechnic University, Hong Kong, China; and Shenzhen Research Institute, The Hong Kong Polytechnic University, Shenzhen, China, e-mail: dangyuan.lei@polyu.edu.hk. http://orcid.org/0000-0002-8963-0193
Guang-Can Li: Department of Applied physics, The Hong Kong Polytechnic University, Hong Kong, China
Qiang Zhang: School of Materials Science and Engineering, Harbin Institute of Technology, Shenzhen, China
Stefan A. Maier: The Blackett Laboratory, Department of Physics, Imperial College London, London SW7 2AZ, United Kingdom; and Fakultät für Physik, Ludwigs-Maximilians-Universität München, 80799 München, Germany

1 Introduction

Metallic nanostructures have played an important role nowadays in materials science and photonic research because they support localized surface plasmons (LSPs) that can strongly confine light into the deep subwavelength volume. Such significant field localization not only results in strong light absorption and scattering enhancement of plasmonic nanostructures favorable for advanced photothermal therapies [1] and high-contrast label-free bioimaging [2] but also produces intense electric fields for boosting various optical effects, such as surface-enhanced Raman scattering (SERS) [3], photoluminescence [4], and coherent nonlinear processes (harmonics generation, four-wave mixing, etc.) [5, 6].

Up to now, various metal nanostructures have been fabricated, including not only individual nanoparticles of different shapes like spheres, rods, and cubes, etc. but also complex constructs formed by rational assembling of two or more individual nanoparticles, such as nanosphere dimers and trimers. The later ones are particularly attractive because they possess narrow gaps that enable more efficient light confinement than the individual constitute particles do and thus provide much stronger field intensities for enhanced light-matter interaction. In addition, the plasmon coupling between constitute particles can produce more diverse and intriguing plasmon modes, which provides more freedom to manipulate the optical properties of assembled nanostructures. Typical examples include bonding and anti-bonding plasmon modes in a metal nanoparticle dimer [7], super-radiant and sub-radiant plasmons in ring/disk nanocavities [8], and plasmonic Fano resonances [9] in metal nanoparticle oligomers. The gapped plasmonic nanostructures are usually

fabricated with lithographic methods. These fabrication methods allow for a flexible design of the nanostructure geometries, but the readily available gap sizes are typically limited to above 15 nm [5]. Self-assembling approach has also been employed to form complex nanostructures. This method allows for fabrication of plasmonic gap size with sub-nanometer scale, but accurate control over the gap size is difficult. Moreover, it is challenging to precisely place active materials (say, quantum emitters) into the nanogaps of such planar structures, which are highly demanded for advanced photonic research and applications, such as cavity quantum electrodynamics [10] and low-threshold nanolasers [11].

The plasmonic nanocavity formed by a closely spaced nanoparticle and metal film, namely a metal particle-on-film nanocavity (MPoFN), seems as a promising platform for plasmon-enhanced spectroscopy (Figure 1) and has been studied intensively in the past years [12–20]. Benefiting from the well-established technologies for thin film deposition and planar spacer fabrication [14, 21], the particle-film gap distance in a MPoFN can be readily controlled for realizing tunable plasmonic properties [12]. The minimal gap size can be even scaled down to the sub-nanometer scale, which makes it possible to study some interesting quantum plasmonic phenomena such as spatial nonlocality [22] and quantum tunneling effect [23]. Moreover, the stacked fabrication procedure largely facilitates the integrating of various active materials into the gaps between the nanoparticles and the metal film, rendering the MPoFN a versatile plasmonic platform that has triggered a series of breakthrough in photonic research and applications, including plasmonic nanolasers at deep subwavelength scale [24], realization of huge spontaneous emission enhancement [25, 26], and more recently, single molecule-light strong coupling at room temperature [27] and single molecule optomechanics in "pico-cavities" [28].

Here, we present a comprehensive review of the nanophotonic researches and applications of MPoFNs. The main content begins with an introduction of the fabrication methods to construct the metal nanoparticle-on-film structures. Then, we summarize the key experimental techniques and tools for optical characterization of the plasmonic responses of individual plasmonic nanoparticle-on-film structures. In the same section, several typical analytical models and numerical methods for studying the optical responses of MPoFNs are also discussed. Subsequently, we discuss the optical properties of various metal film-coupled nanostructures in great detail, followed by several sections reviewing their wide spectrum of applications in plasmon-enhanced Raman spectroscopy, spontaneous emission, as well as photocatalysis and molecular nanochemistry. Finally, we conclude the review by a prospective of this kind of compact nanocavities in future nanophotonic researches and applications.

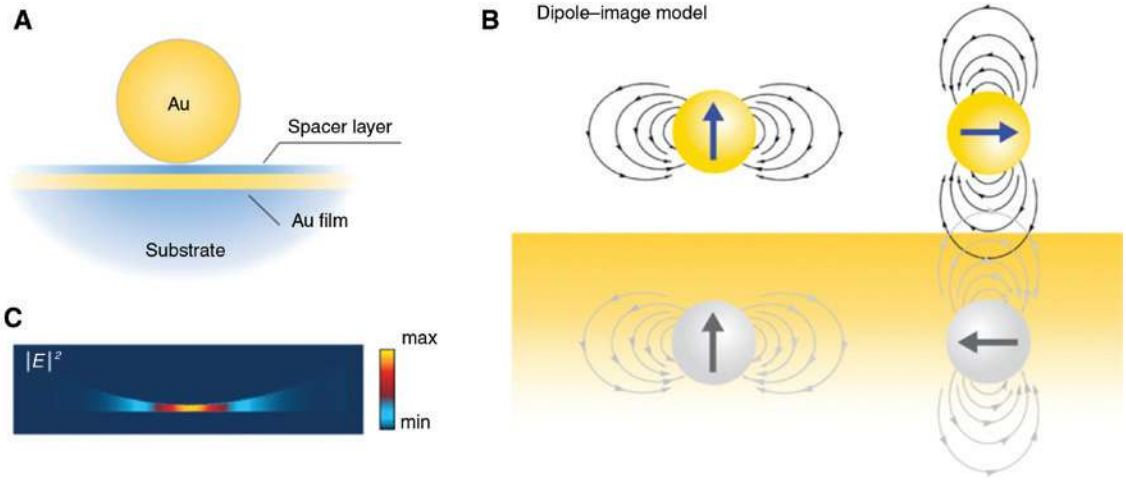

Figure 1: Plasmonic nanocavity formed by closely spaced metal nanoparticles and film.
(A) Schematic of single nanoparticle-on-film construct. (B) Schematic illustration for the plasmon couplings in single nanoparticles on film within the dipole approximation. (C) Simulated field intensities for a single gold nanoparticle coupled to film show strong field localization in the gap region. The gold nanosphere is 100 nm in diameter and spaced from the film by a 1-nm-thick dielectric layer with a refractive index of 1.5. The excitation source is set by a plane wave glancing at the film with polarization oriented in the incidence plane.

2 Fabrication of MPoFNs

In plasmon-enhanced spectroscopy applications, flexible manipulation of the plasmonic resonances of metal nanostructures is often required to attain optimal light-mater interactions, such as spectrally or spatially overlapping with active materials [29]. These spectral or spatial manipulations are typically achieved by engineering the geometry and composite of the plasmonic nanostructures or the dielectric index of the ambient media. Particularly, for the nanostructures closely separated from a large enough metal film, the plasmonic properties of the whole system are dominantly determined by the strong plasmon coupling between the real nanostructures and their corresponding images in the metal film. This suggests that precise control of the gap distance between the nanoparticles and the underlying metal film is crucially important. In this section, we particularly focus on the fabrication technologies of thin spacers that have been developed for achieving reliable control over the particle-film gap distances scaled down to the sub-nanometer scale.

For the simplest case in which a single nanoparticle is coupled to a metal surface (Figure 1A), two fabrication configurations have been frequently employed to insulate them from each other. One of these two configurations is to separate the nanoparticles from the metal film by inserting a thin planar dielectric layer in between them, as schematically indicated in Figure 2A. The other one, however, uses a dielectric shell coating around the nanoparticles to avoid direct contact with the underlying film (Figure 2B). Within the frame of these two configurations, various solutions have been developed for precise controlling of the gap distance in metal film-coupled nanoparticles.

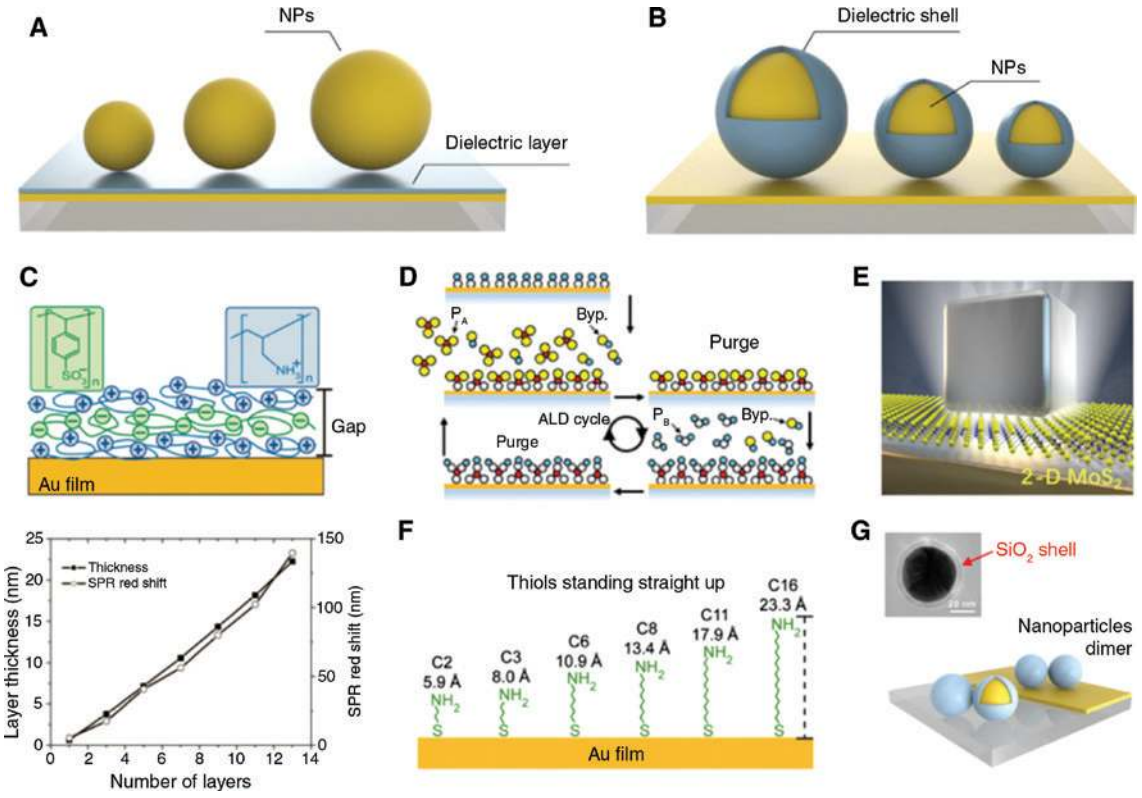

Figure 2: Methods and technologies to create nanometric-thick gaps in metal nanoparticle-film cavities.
(A) Schematic of nanoparticles separated from a metal film with thin planar dielectric layer sandwiched in between them. (B) Schematic of dielectric shell-isolated metal nanoparticles on film constructs. (C) Schematic illustration of the LBL method (upper) for spacer fabrication and the fabricated film thickness as a function of the number of layers (bottom). Extracted from [12]. (D) Illustration for inorganic dielectric film deposition for thickness controllable spacer by the ALD method. P_A (P_B) refers to precursor A (precursor B), while "Byp." is short for byproduct. Redrawn from [30]. (E) Layered 2D materials act as the spacer between the nanoparticles and the underlying film. Extracted from [31]. (F) Gap distance control with the SAMs of amine-terminated alkane thiols of different chain lengths. The spacer thickness is determined by the chain length and thus depends on the number of chained carbon atoms. Extracted from [21]. (G) Electronic scanning micrographs of the metal nanoparticles coated by sub-nanometer-thick dielectric shell (upper) and schematic of the metal film-coupled nanoparticles dimers (bottom). Partially redrawn from [32].

As for the planar spacer fabrication, a well-developed solution is the layer-by-layer (LBL) method, as schematically described in Figure 2C. The principle of such LBL method is to deposit the poly-electrolyte (PE) spacer consisting of alternating monolayers of positively charged poly-(allylamine) hydrochloride (PAH) and negatively charged polystyrene sulfonate [33]. Since the thickness of each PE monolayer is constant, the total thickness of the spacer is determined by the number of the monolayers deposited. Note that all LBL depositions are initiated and terminated with a PAH monolayer to facilitate both the attachment of the bottom layer to the underlying gold film through amine-gold interactions and the electrostatic stabilization of the negatively charged gold nanoparticles to the top PE layer [21]. Ellipsometry measurements indicate that the readily obtainable spacer thicknesses with this method are typically in the range of 2–20 nm (bottom in Figure 2C). Similar to the LBL approach, fabrication of nanoscale-thick inorganic spacers has also been demonstrated by using the top-down approach, particularly the atomic layer deposition (ALD) method [30]. Spacer thickness control is achieved by launching a different number of ALD circles. As illustrated in Figure 2D, only one molecule layer is deposited on the substrate in each ALD circle. The final spacer thickness is thus dependent on the number of layers or ALD circles. With this well-established planar deposition technology, fabrication of robust inorganic material spacers (Al_2O_3, MgF_2, etc.) with controllable thickness at the nanoscale has been realized [24, 34]. For example, a planar SiO_2 layer as thin as 2 nm has been demonstrated as a spacer separating the gold nanoparticles and the metal film [14]. To fabricate spacer layers with thickness approaching the sub-nanometer scale, i.e. ranging from a few angstroms to a few nanometers, a method using self-assembled monolayers (SAMs) of amine-terminated alkanethiols with different chain lengths has been proposed [21, 22]. As indicated in Figure 2F, the spacer is formed when the alkanethiol molecule monolayer is self-assembled on the metal surface. Its thickness depends on the length of individual alkanethiol molecules, which is determined by the number of constituent carbon atoms. By employing alkanethiol molecules with different numbers of carbon atoms, the monolayer thickness can be precisely controlled within the length range of 0.5–2 nm. Such ultrathin layer spaced nanoparticle-film constructs are highly demanded because they show great potential as candidate platforms to address quantum plasmonics such as quantum tunneling and nonlocal effects [35–37]. Two-dimensional (2D) materials, such as graphene and layered transition metal dichalcogenide semiconductors, have been recently demonstrated as natural yet promising candidates for fabrication of ultrathin spacers, for example as shown in Figure 2E [38, 39]. Due to the atomic thickness of the monolayered 2D materials, the obtainable spacer size can be scaled down to a few angstroms. Similar to the LBL approach, incremental layer numbers of such 2D materials can expand the gap size to a larger scale, typically a few nanometers, fabricated with the mechanical exfoliation or chemical vapor deposition methods. For details of the synthesis methods of layered 2D materials, interested readers may refer to [40, 41].

When nanoparticles coated with dielectric shells are directly deposited on a metal film, the gaps between the nanoparticles and the metal film are naturally formed with gap distances totally determined by the thickness of the coating shells (Figure 2B). Therefore, tuning the particle-film gap sizes can be simply realized by controlling the shell thickness, and the solutions once developed for controlling the interparticle distances in nanoparticle dimers can be seamlessly applied here [42, 43]. Previous studies using this approach have demonstrated tunable particle-film distance down to 1 nm scale with silicon dioxide shell [44]. Besides, in constructing more complex plasmonic constructs with metal films involved, this shell-isolation configuration may be the only solution. As in the film-coupled nanoparticle dimer (Figure 2G), the dielectric shell enclosing the nanoparticle elements guaranties the insulating near-field coupling between different metal parts, and thus the formation of multiple field hot spots residing in particle-particle and particle-film nanogaps. Such composite plasmonic constructs with multiple nanogaps, as will be discussed later, usually exhibit sensitive polarization-dependent optical properties, which enables selective activation of emitters inside the different gap regions [32, 45, 46].

In the aforementioned approaches for tuning nanoparticle-film gap distances, the structure geometries are fixed once the fabrication ends. This greatly hinders the dynamic control of their optical properties, which is unfavorable in some *in situ* spectroscopy applications. Nevertheless, metal nanoparticle-on-film constructs with dynamically controllable gap distances have been demonstrated in a few past studies [17, 47–49]. One of them uses the direct current (DC) electric field to drive the nanoparticles toward or away from the underlying metal film (Figure 3A). However, this approach requires that the nanoparticles are negatively charged with specified surfactant decorations. For dynamic spacer control of neutral nanoparticles above metals, methods based on the electrochemical oxidization of reactive metals like aluminum (Al) have been developed [47, 49]. In these solutions,

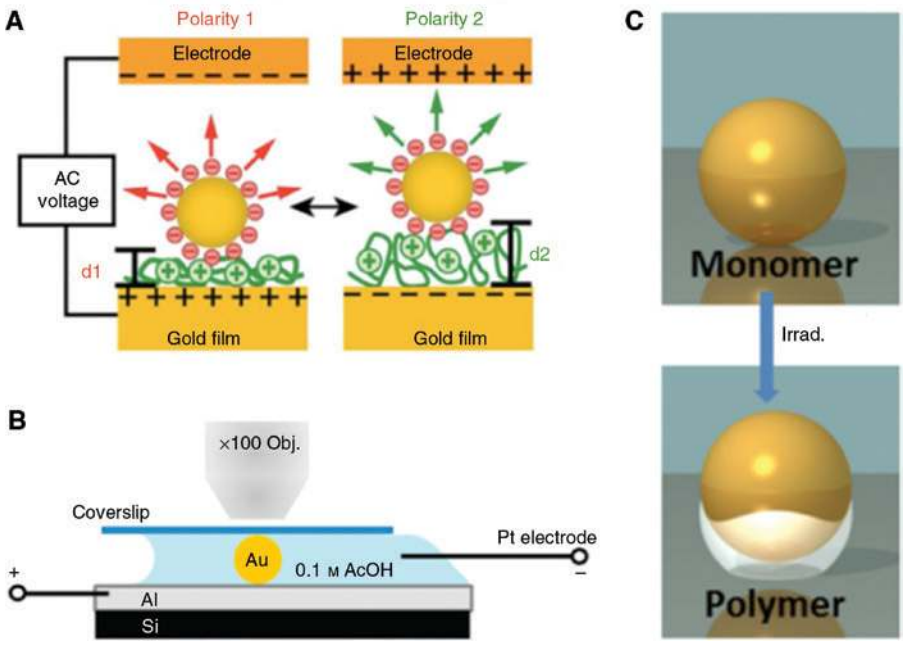

Figure 3: Dynamic control of the gap distance between metal nanoparticles and the film.
(A) Schematic of nanoparticles driven toward or away from the underlying film upon applying an external electric field across the gap junction. Extracted from [17]. (B) Controllable electrochemical oxidization of the metal surface to form a dielectric layer, which gradually separates the particles from the metal substrate. Extracted from [47]. (C) Plasmon-induced polymerization of the monolayer polymer on metals expands its volume upon light irradiation, progressively driving the particles away from the metal film. Extracted from [48].

the spacer layers are progressively formed at the metal surface through electrical oxidization (Figure 3B), and the resultant spacer thickness can be readily controlled by the oxidization conditions, such as the applied electric field intensity, immersion composite, etc. Besides electrical control approaches, light irradiation can also act as a stimulus to trigger the controllable gap forming at the particle-film contact. A representative of such methods is the so-called plasmon-induced polymerization [48]. As depicted in Figure 3C, upon laser irradiation, the thiophenol SAM (~0.6 nm thickness) on the Au substrate expands its volume and thereby progressively increases the gap distances. While increasing the gap distance results in a continuous blue-shift of the gap plasmon resonance, it is interesting to find that the monolayer polymer growth terminates when the resonance spectrally shifts to the irradiation wavelength. Such self-limiting mechanism can provide a programmable way to tune the plasmon resonances of gapped nanostructures by simply selecting the irradiation wavelength.

Another important concern in constructing MPoFNs is the metal surface roughness. The plasmonic responses of MPoFNs can be modified by poor film roughness, which produces local morphology distortion in the nanocavities. The resulting deviation from design geometries inevitably degrades the functional performances of nanodevices or components based on MPoFNs [13]. The root-mean-squared (RMS) roughness of metal films deposited by readily accessible technologies and methods such as sputtering, thermal/electric evaporation and pulsed laser deposition, etc. [50], is typically a few nanometers [51]. To further improve metal film quality, the template-stripping method was developed by Butt et al. [52, 53] and Hegner et al. [54] and recently applied in the fabrication of MPoFNs [39]. Taking gold film deposition as an example, a schematic illustration of the template-stripping process is presented in Figure 4A. Firstly, the gold film is deposited onto a naturally flat template by common evaporation methods. The templates can be mica or polished wafers, which are cleaved along the crystal directions and thus possess an atomically smooth surface. Then, a mechanical support (silica, for example) is glued onto the metal film through the spin-coated epoxy layer. Finally, the original deposition substrate is peeled off, leaving an ultrasmooth gold surface with roughness comparable to the template. Obviously, this process allows for the preparation of atomic smooth metal surface with large areas, which are solely limited by the size of the template materials. Previous studies reported a measured RMS roughness of 0.2 nm for template-stripped gold films, largely surpassing the thermally evaporated ones (right column in Figure 4B), with a typical RMS roughness of ~1.45 nm

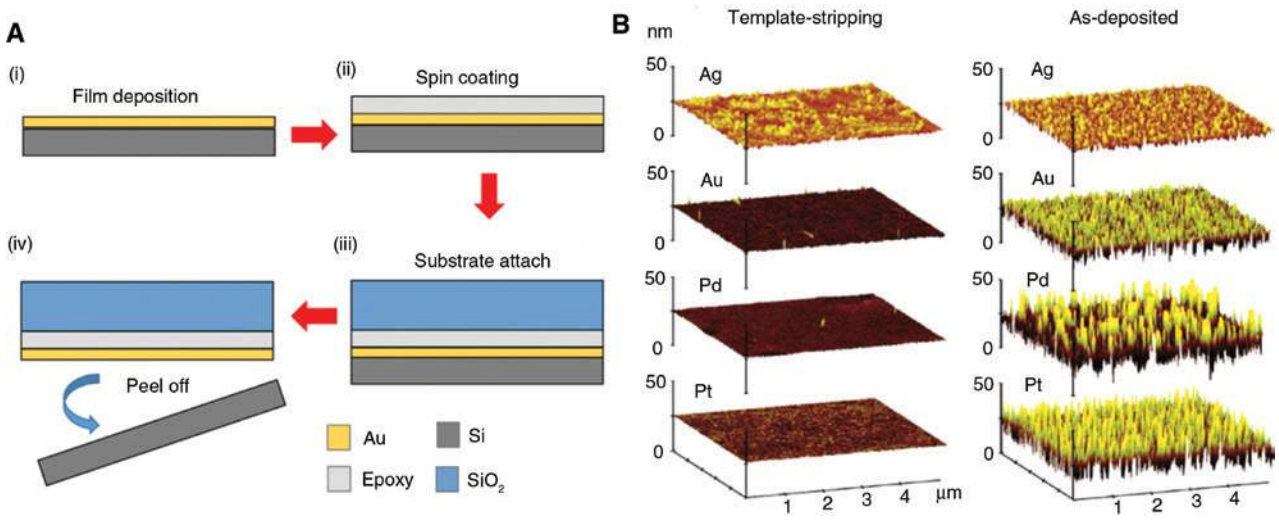

Figure 4: Template-stripping method for fabrication of atomically smooth metal films.
(A) Schematically illustrated fabrication procedure of template-stripping method, taking the gold film for example. (B) Comparisons between the surface roughness of metal films fabricated with template-stripping method and common deposition methods (thermal/electric evaporation, etc.). Extracted from [54].

[55]. As indicated in Figure 4B, significantly improved film roughness has also been demonstrated for several other metals (Ag, Pd, Pt, etc.) by using this template-stripping method [56].

An additional benefit with this method is the capability to store the metal film in the sandwich configuration without inducing any contaminations to the gold surface. As shown in step (iii) in Figure 4A, the gold film is sandwiched in between the template and support layers, which prevents the metal surfaces from being exposed to ambient environment [57]. Therefore, fresh gold films can be obtained on demand by cleaving the sandwiched structures. Note that the metal nanoparticles are typically fabricated using chemical synthesis methods and thus possess crystallized-structure bonded surface roughness [58]. Although the single-crystalline metal film flakes have also been demonstrated with chemistry-based approaches [59, 60], the obtainable film sizes are small, typically limited to the micrometer sized scale.

3 Optical characterization and analytical tools

Characterizing MPoFNs by some near-field probe approaches such as electron energy loss spectroscopy and scanning near-field optical microscopy is usually problematic. This is because the field hot spots in MPoFNs are mainly confined in the gap regions between the nanoparticles and the metal films, where the near-field nanoprobes cannot be accessed. Thus, studying the plasmonic responses of these cavity structures heavily relies on some invasive techniques, such as far-field optical spectroscopy. Particularly, the dark-field microscopies have become an indispensable tool to investigate the optical properties of individual plasmonic nanostructures *via* inspecting their scattering responses. With polarization-resolved dark-field spectroscopy, not only the radiative plasmon modes can be directly identified, but also some dark modes can be captured by properly configuring the illumination condition [61]. Individual plasmonic nanostructures with asymmetric geometry usually exhibit polarization-dependent optical responses, which means that different plasmonic modes can been excited only by the specified incidence polarizations [62]. In the individual metal film-coupled nanoparticles, the gap plasmon mode originating from the vertical bonding between the nanoparticle dipole and its induced one in the film can produce the strongest field localization in the gap. Therefore, excitation of such gap mode is highly desired in plasmon-enhanced applications, such as the Raman scattering [63], spontaneous emission [29], and nonlinear optical effects [64].

In the standard optical dark-field microscopy systems, incoherent white lights are widely used to illuminate the nanostructures samples (left in Figure 5A). This standard white light illumination permits optical examination of the plasmonic responses in a wide spectral range. However, the unpolarized features of the illumination

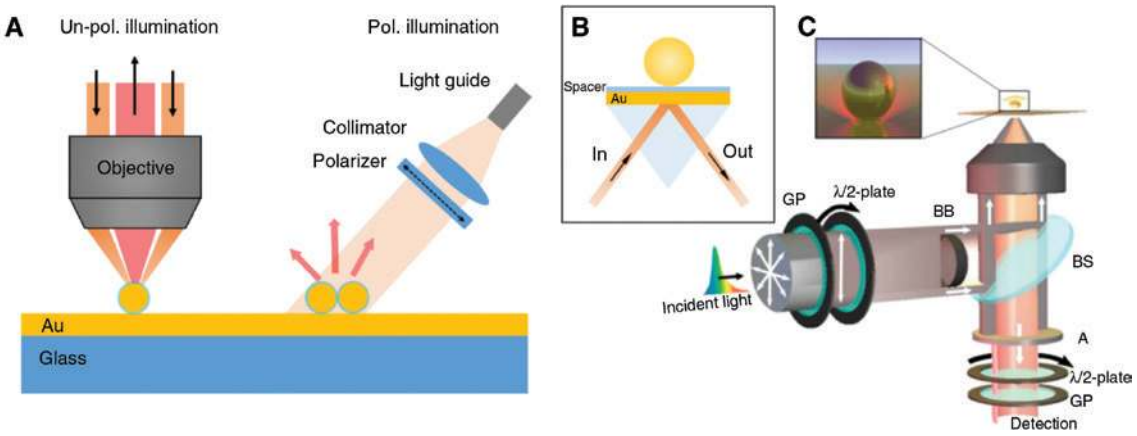

Figure 5: Illumination configurations for excitation of the particle-film gap plasmons in metal film-coupled nanostructures. (A) Schematics of the illumination configuration in standard dark-field microscopy systems (left) and oblique incidence arm constructed for polarization controllable illumination (right). Extracted from [62]. (B) Excitation of the gap plasmons with propagating surface plasmons generated at metal surfaces. (C) Dark-field microscopy system integrated with a coherent light source generates pure in-plane polarization in the focal plane. The orientations of the in-plane polarization can be tuned by rotating the broadband half-wavelength ($\lambda/2$) plate inserted in the excitation path. Extracted from [65].

enable simultaneously exciting multiple plasmon modes polarized in different directions, thus making it difficult to resolve the physical origins of distinct plasmon resonances. Due to the large focusing cone of the dark-field objectives, even pre-polarized incidence, for example light beam filtered by a liner polarizer, can be severely distorted when reaching the focal plane [62]. To address this issue, improved dark-field illumination configurations with polarization controlling modules have been developed and integrated into the standard microscopy platforms [20, 62]. A representative is depicted in Figure 5A (right column). The incidence polarization of the beam from the illumination arm can be continuously tuned between the in-plane (parallels to the substrate) and out-of-plane (nearly parallels to the substrate norm) states. This illumination configuration is particularly suitable for characterizing the gap plasmon modes supported in MPoFNs because these modes are most efficiently excited upon the out-of-plane polarization illumination, which, however, is usually mixed with the in-plane polarization and takes a small intensity proportion of the illumination in the standard dark-field microscopy platform. The vertical gap modes in metal nanoparticle-film constructs can also be preferentially excited with the near-field configuration, which utilizes the propagating surface plasmons at metal surfaces (Figure 5B) [17, 66]. Beyond the interband transition band of metals, the out-of-plane polarization components of propagating surface plasmons near the metal surface can be significantly stronger than their in-plane counterparts (with a typical amplitude ratio 2 for gold above 600 nm). Such field characters of surface plasmons near the metal surface thus render the near-field illumination configuration favorable for excitation of the vertical gap modes. However, in some studies, pure in-plane polarizations are preferred for studying the in-plane asymmetric properties of plasmonic nanostructures, while simultaneously requiring the exclusion of out-of-plane responses. The creation of such kind of polarization states in the focal plane has been demonstrated by using coherent white light lasers. As illustrated in Figure 5C, the out-of-plane field components with defined polarization directions exist in the focused beam but suffer destructive interference in the focal plane, leaving the pure in-plane polarization field components. The pure in-plane polarization can be oriented by simply rotating a half-wavelength plate inserted in the excitation path [65]. Such polarization configurations are particularly suitable for studying the transverse plasmon couplings in the metal particle-film nanocavities [19, 65, 67–69].

The above concerns in dark-field spectroscopy of single nanostructures also exist in laser-based spectroscopy applications, e.g. fluorescent imaging and nonlinear optical spectroscopy. Efficient excitation of the gap plasmons in MPoFNs for strong field enhancement is not readily available in laser-based spectroscopy because the commonly used laser beams are transversely polarized. Although the focused laser incidence striking the individual nanostructures can be set off-axis to increase the amplitude proportion of longitudinal field component (similar to that in Figure 5A) [23], the excitation efficiency is quite low. Besides, the difficulties in its optical alignment hinder it readily integrated to the

common spectroscopy platforms. To address this issue, laser beam engineering based on vectorial optics has been utilized to tailor the polarization states (Figure 6A) [70–72]. It has been found that the longitudinal field intensity dominates the total field intensities in the focal plane after focusing a radially polarized laser beam [73]. Obviously, this beam configuration can be utilized to preferentially drive the longitudinal polarization-sensitive optical processes [74] and efficiently excite the gap plasmons in the metal film-coupled nanostructures for enhanced light-matter interactions [75]. Another easy-to-perform solution for increasing longitudinal field intensity in the excitation is using highly focused scalar laser beams [71, 76, 77]. Taking a linearly polarized beam as an example (Figure 6C–E), when focused by an objective with moderate numerical aperture (NA), a small fraction of longitudinal field component emerges in the focal plane. This depolarization effect also holds true for other incidence polarizations (circular polarization, etc.) and vectorial beams. Generally, the intensity weight of these nontransverse components in the total power largely depends on the NA of the focusing objectives (Figure 6D). Larger objective NA means more power energy transformed into the longitudinal field components in the focal plane. Thus, objectives with large NA are favorable for prompting the excitation efficiency of the gap plasmons in MPoFNs.

In addition to experimental characterization of MPoFNs, analytical models and numerical tools are often required to help in understanding the observed plasmonic responses. Besides the dipole-image model within electrostatic approximation (depicted in Figure 1B), an approach based on the multiple scattering process [78, 79] (Figure 7A) has been introduced to describe the fundamental optical properties of substrated nanoscatters. The main idea of this approach is that the total electromagnetic waves within the domain enclosing the scatters can be decomposed into four wave components: incident wave V_I, reflection of the incidence by film without the nanoparticle V_{IR}, scattered wave from the nanoparticle W_S, and the reflection of scattered wave from the nanoparticle by the metal film V_{SR}. With introduction of the scalar Debye potential to represent the field components, a complete analytical solution can be derived to account for the far-field plasmonic responses of individual nanoparticles on film.

Another analytical approach for determining the plasmon resonances of the individual MPoFN is the generalized circuit model developed by Felix Benz et al. [80]. By introducing a high-frequency circuit composed of

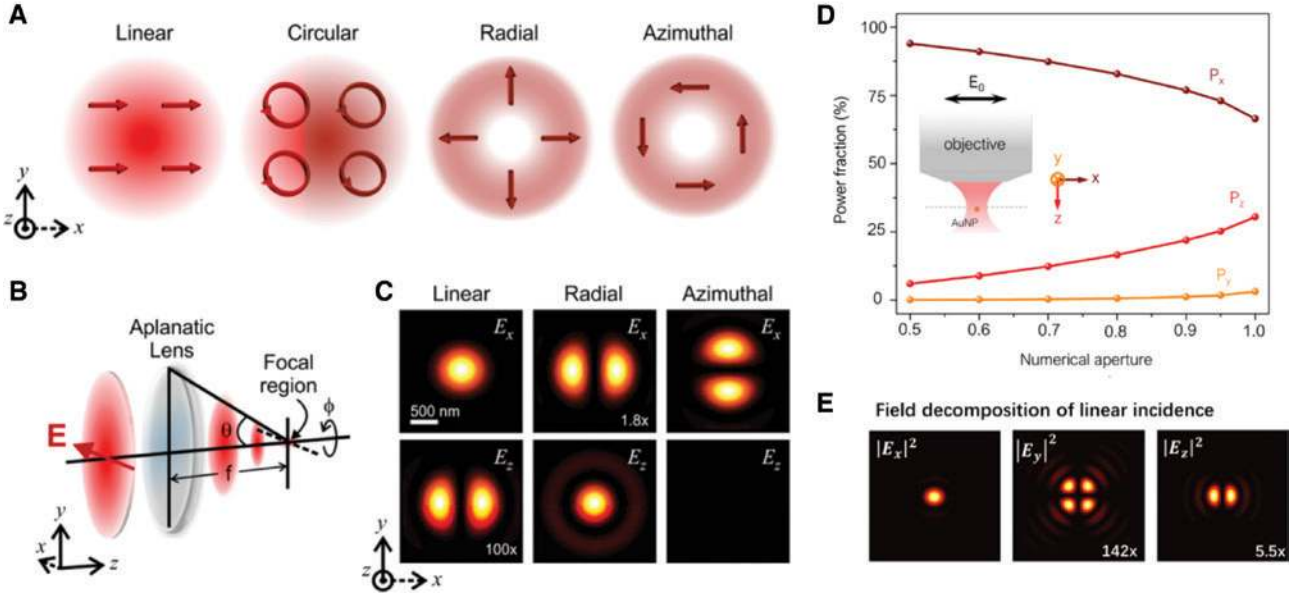

Figure 6: Field intensity distributions in the focal plane of a microscope objective.
(A) Intensity profiles of various laser beams without focusing. The arrows indicate the local polarization directions in the beams. (B) Simplified schematic of the typical focusing system in optical spectroscopy setups. (C) Focal field distributions of various beams when focused by an aplanatic lens. Extracted from [70]. (D) Correlation between the numerical apertures of objectives and the power of each field component generated in the focal plane. (E) Calculated intensity patterns of the three orthogonal field components in the focal plane for a linearly polarized incidence. The objective numerical aperture used is 0.95 and the light wavelength is 850 nm.

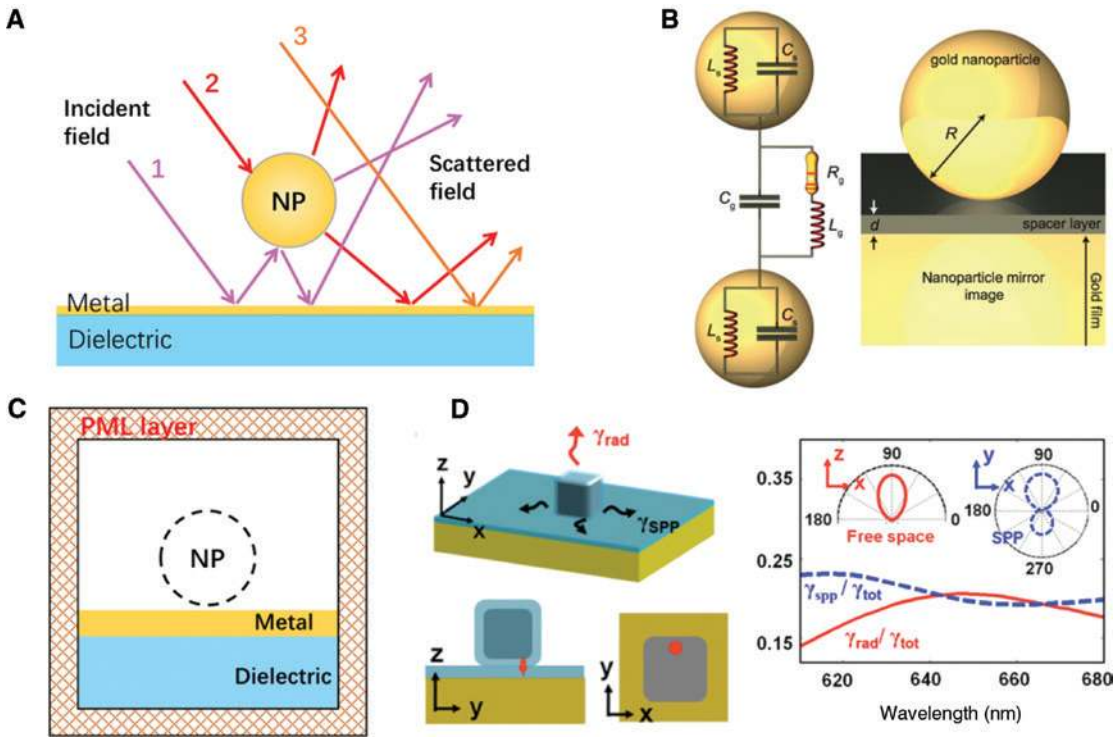

Figure 7: Analytical models and numerical methods for analysis of the optical responses of metal film-coupled nanoparticles. (A) Schematic illustration of the multiple scattering process occurring in the metal film-coupled nanostructures. (B) An equivalent circuit model for describing the nanoparticle-film gap plasmon oscillations. Extracted from [80]. (C) Simulation configurations for substrated-nanostructures with the two-step strategy. The nanoparticle is set invisible in the first simulation step to calculate the background field, which is then used to excite the complete structure. PML is short for perfect matching layer. (D) Near-to-far-field transformation approach developed to extract the angular patterns of both the free-space radiation and the guided modes. The figure in the left column illustrates the radiation dynamics for nanostructures atop layered substrates excited by a dipole source. The right figure shows the free-space (red) and guided-mode (blue) radiation patterns of the structures in the left figure, as well as their spectra of radiative decay rates. Extracted from [81].

inductors, resistors, and capacitors (Figure 7B), a simple analytical expression for describing coupled plasmon systems can be derived. This model can not only predict the resonance wavelength of coupled plasmonic cavities with both the conductive and capacitive interactions but also reveals the scaling rules of the plasmon resonances of coupled plasmon systems.

The aforementioned models offer qualitative, even quantitative, descriptions of the plasmon resonances supported in MPoFNs and make it possible to derive analytical results in line with the experimental observations. However, the applicable nanoscatters are limited to MPoFNs comprising of single nanoparticles with simple geometries such as nanospheres. The plasmon hybridization (PH) model proposed by Peter Nordlander and coauthors [82, 83] has been frequently utilized to describe the plasmon coupling interactions in complex nanostructures. As a close analogy to the atoms forming a molecule, the plasmon response of coupled plasmonic nanosystems can be understood by the PH between the elementary plasmons supported by constitute nanoparticles. Although this treatment is physically intuitive, the currently available quantitative solutions for coupled plasmonic nanostructures are limited to several geometries [83–85], nanosphere dimers, core-shell nanospheres, etc., largely because of the difficult mathematical treatments for geometries with greater complexity. As for MPoFNs, the complete analytical solutions by the PH model had been found only for the single nanoparticles case [86]. Moreover, the PH model still relies on numerical simulations to derive the optical properties of plasmonic nanostructures. Transformation optics (TO), developed by John Pendry et al. [87, 88], provides a powerful tool to analytically solve coupled plasmon problems. By conformal mapping, the complex plasmonic nanostructures of interest can be transformed into a simpler plasmonic system that can be solved analytically. Although the TO approach offers unique physical insight of surface plasmons in coupled nanostructures, it readily works within the electrostatic approximation (i.e. applicable to small

nanosystems) and mostly applies to planar nanostructures [89–92]. Thus, revisits of the metal nanoparticles coupled to film system with TO are currently limited to cases of relatively small nanoparticles [93] and nanowires on metal surface construct in which a 2D analytical frame was adopted [94].

In light of the above concerns, full-wave numerical simulations based on finite difference time domain and finite element methods (FEM) are widely utilized to assist the understanding of experimentally observed optical responses of plasmonic nanostructures [95, 96]. Being different from the isolated plasmonic entities, the single metal film-coupled nanostructures involve a finite-sized component (i.e. the nanoparticle) and an infinite large metal substrate. Taking a commercial FEM simulation package, COMSOL Multiphysics, as an example, it calculates the optical response of a scatter with a predefined background field, typically a plane wave in homogeneous media. However, when dealing with layered structures, for example with an infinite large substrate being present, the background field in the calculation domain will no longer be a plane wave due to the reflection and transmission at the surface of the substrate. A compromised treatment to this issue is using a two-step simulation configuration [19]. As depicted in Figure 7C, in the first simulation step, the background field is calculated with the absence of the nanoparticle. Then, the nanoparticle is set active in the second step, and the background field obtained in the first step is then used as the excitation to calculate the scattering field. Based on the scattering field, not only the spectral responses can be calculated, but also the angular radiation distribution can be derived with a near-to-far field transformation approach based on reciprocity arguments (Figure 7D) [81].

4 The fundamental plasmonic responses

The linear optical properties of individual MPoFNs are largely determined by their plasmon resonances, which can be usually identified from the far-field scattering responses. Dark-field spectroscopy indicates that the scattering responses of film-coupled nanostructures are dominantly determined by the dipolar plasmon couplings between the nanoparticle and the underlying film. Within the dipole approximation (as illustrated in Figure 1B), a vertical bonding dipole plasmon (V-BDP) mode emerges when the vertically polarized nanoparticle dipole couples to its induced dipolar charges in the underlying film. This V-BDP mode is featured with significantly enhanced radiation efficiency with respect to that of the single particle, typically manifested by a prominent resonance peak in the scattering spectrum as well as a doughnut-shaped scattering pattern (Figure 8A). Likewise, the transversely polarized nanoparticle dipole would induce an image dipole underlying film but with opposite polarity, resulting in a transverse bonding dipole plasmon mode with suppressed radiation. Because of these distinct dipole bonding directions, MPoFNs exhibit polarization-dependent plasmonic responses [62]. As indicated in Figure 8B, different plasmon modes can be selectively excited with specified incidence polarizations. Beyond the dipole approximation, the high-order modes in the film-coupled nanoparticles have been ambiguously identified in experiments but remain too weak to be resolved [78]. Changing the nanoparticle size or the particle-film gap distances can modify the plasmonic response of MPoFNs (Figure 8C–D). Particularly, the V-BDP modes are shown to have extraordinarily high sensitivity to the gap distances. Even sub-nanometer scaled decreasing of the nanoparticle-film distance can significantly red-shift the resonance within the visible-near-infrared spectral range, accompanied by an intensified field localization within the tighter gap nanocavity. However, the red-shifting and field localization of the V-BDP modes are limited by nonlocal [22, 37] and electron tunneling [23, 98] effects emerging at extremely narrow gap distance (say, <1 nm).

Due to radiation losses, the dipolar plasmon modes of single metal nanoparticles usually possess broad resonance linewidth. It was found that placing the aluminum nanoparticles near the metal surface can significantly reduce the scattering resonance linewidth (Figure 9A), thus improving the quality factor of the plasmonic cavity [99]. It has been confirmed that such resonance linewidth narrowing is caused by the reduced radiation loss resulting from PH between the electric dipole and quadrupole modes. This linewidth shrinking is also predicted for other metal nanoparticles when placed atop a metal substrate but is not noticeable for gold due to its lower plasma frequency (Figure 9B) [17]. Nevertheless, pronounced resonance linewidth shrinking was observed for gold nanoparticle dimers on film (Figure 9C) [32]. Besides the reduced radiation loss, it was found that the red-shifting of the dimer resonance beyond the interband transition band largely reduces the nonradiative loss, thus leading to much narrower resonance linewidth compared to that for the nanoparticle monomers on film.

It is worth noticing that the local nanogap geometries and the gap contents can also dramatically modify the plasmonic responses of MPoFNs. It is well understood that

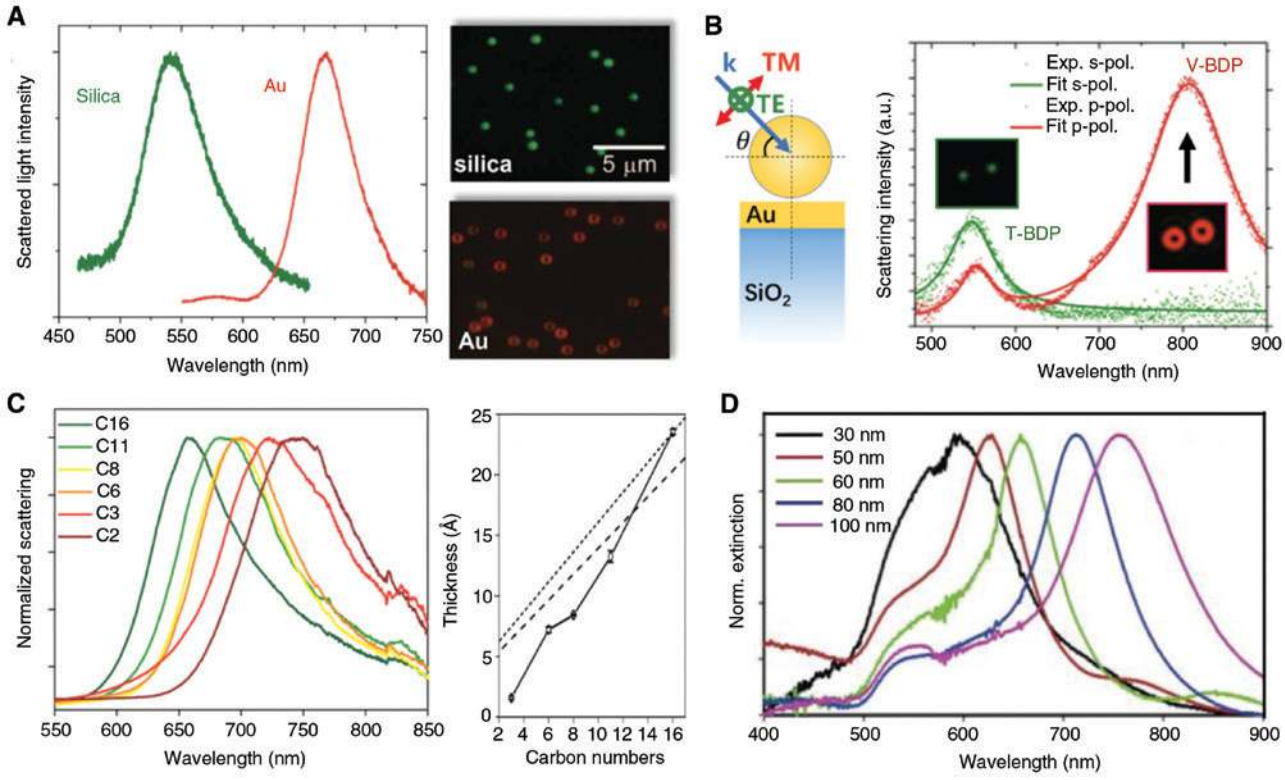

Figure 8: Fundamental plasmonic responses of metal film-coupled nanoparticles.
(A) Comparisons of scattering spectra (left) and dark-field scattering patterns (right) of 60 nm gold nanoparticles deposited on silica (green) and gold film (red), respectively. Extracted from [12]. (B) Distinct optical properties of individual metal nanospheres on metal film upon light excitations with different polarizations. Insets show the far-field radiation patterns of each plasmon mode, with the corresponding resonance position indicated nearby. Partially extracted from [62]. (C) The particle-film gap distance dependent gap plasmon resonances. The C2, C3… mark the incremental spacer thickness in the form of carbon numbers, with large number for thicker spacer. The plot on the right shows the correlation between the carbon number and the corresponding spacer thickness. Extracted from [21]. (D) Nanoparticle size dependence of the gap plasmon resonances. Redrawn from [97].

the gap plasmon resonances exhibit high sensitivity to the refractive index of the spacer materials, where strong field localization occurs [100]. Besides, the conductivities of the gap contents (conductive molecules, graphene, etc.) are shown to impact the plasmon coupling. For a plasmonic nanoparticle dimer directly deposited on metal surface, electrically connecting between the constitute nanoparticles *via* the conductive substrates can produce the so-called charge transfer plasmon (CTP) mode [101, 102], featured with a dipolar nature formed by two monopoles with opposite charges in the nanoparticle dimer (Figure 10A–B). More generally, the conductive bridging between the nanoparticle and the underlying film can be switched on and off by properly selecting the spacer materials with different conductivities. It has been reported that a strong 50 nm blue-shift of the gap plasmon resonances can be obtained by replacing the gap-hosted insulating molecules with a chemically equivalent conductive version differing by only one atom (Figure 10C) [103]. With photochromic molecules incorporated into the gap region, a dynamic control of the gap junction conductivities has been recently demonstrated in the metal film-coupled nanoparticles [104]. When exposed to an ultraviolet (UV) light environment, the gap plasmon resonance exhibits a large blue-shift even surpassing the resonance linewidth (~71 nm), corresponding to an on/off ratio up to 9.2 dB and a tuning figure of merit up to 1.43.

In addition to the plasmon resonances resulting from plasmon couplings, waveguide-like resonances emerge in the narrow particle-film gap cavities, when the film-coupled nanoparticles do not have a point-contacting interface facing the gap, such as nanorods [105, 106], faceted nanospheres [107], and nanocubes [19]. These modes show similar local field profiles with those of transverse plasmon cavity modes sustained by optical metal-insulator-metal patch antennas [108, 109]. Different from the antenna modes produced by longitudinal plasmon coupling between the nanoparticle and

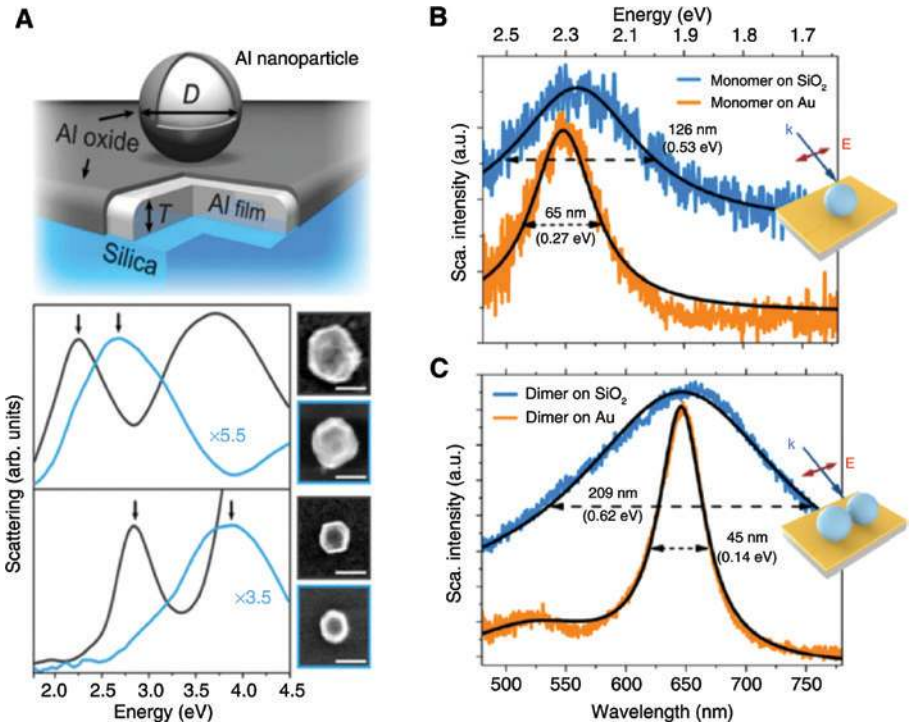

Figure 9: Metal substrate-induced linewidth narrowing of nanoparticle plasmon resonances.
(A) Aluminum nanoparticles closely separated from metal film (black curves) result in reduced resonance linewidth with respect to its counterpart on silica (blue curves). This effect can be more evidently observed for larger nanoparticles. The lower two panels show the scattering spectra of differently sized aluminum nanoparticles (180 nm and 100 nm) on aluminum film and silica substrate. Extracted from [99]. (B) Comparison of the resonance linewidth of gold nanoparticle monomer on silica (blue) and gold film (orange). The metal film-induced linewidth narrowing seems not so pronounced for the gold nanoparticle monomer. The inset illustrates the light excitation configuration. (C) Replacing the silica substrate of the gold nanosphere dimer significantly reduces its plasmon resonance linewidth. The individual gold nanoparticle monomers are 100 nm in diameter and coated by a cetyltrimethylammonium bromide (CTAB) layer with thickness ~1 nm. Extracted from [32].

underlying film, these cavity modes exhibit much lower radiation efficiency and can tightly confine energy into the nanocavities. Nevertheless, the PH of antenna modes and cavity modes enables the observation of these dark modes in the far-field scattering (Figure 10D). Besides, it has been found that these cavity modes can be strongly modified by the particle-film gap distances and the size of the plane facing metals rather than the nanoparticle size [107]. This exquisitely sensitive-to-gap morphology allows for tracing atomic-scale changes in the nanogaps. Monitoring the light-induced atom reconstruction process has been successfully demonstrated by tracing the evolution of the cavity mode resonances in scattering [67], and even the induced structural asymmetry can be revealed through analysis of their polarization responses (Figure 10E) [65]. In the film-coupled nanoparticles with facets, the external UV radiation can drive the atom migration toward the particle bottom. Such migration of atoms would not only increase the facet size but also can cause the formation of a metal protrusion progressively approaching the underlying film, particularly when the spacer content is not so robust. With continuous irradiation, the protrusion finally contacts the film, forming a metal filament electrically connecting the particle and the underlying film. This geometry transition can dramatically affect the hybridization of the plasmonic antenna modes and the transverse cavity modes, thus enabling real-time tracking of the optical welding process through the groove cavity modes in plasmonic nanocavities [110].

Importantly, the lowest-order cavity modes in MPoFNs can be attributed to magnetic dipolar modes that show strong confinement of magnetic fields inside the particle-film nanogaps (Figure 11A). This magnetic response has been particularly addressed in faceted nanospheres, relatively large metal spheres [112, 113], and nanocubes [19] when all coupled to a metal film, as well as rectangular patch nanoantennas [114]. Specially, in large metal spheres on film, this magnetic mode can be spectrally tuned to overlap with the broad particle transverse dipole mode, which leads to pronounced Fano

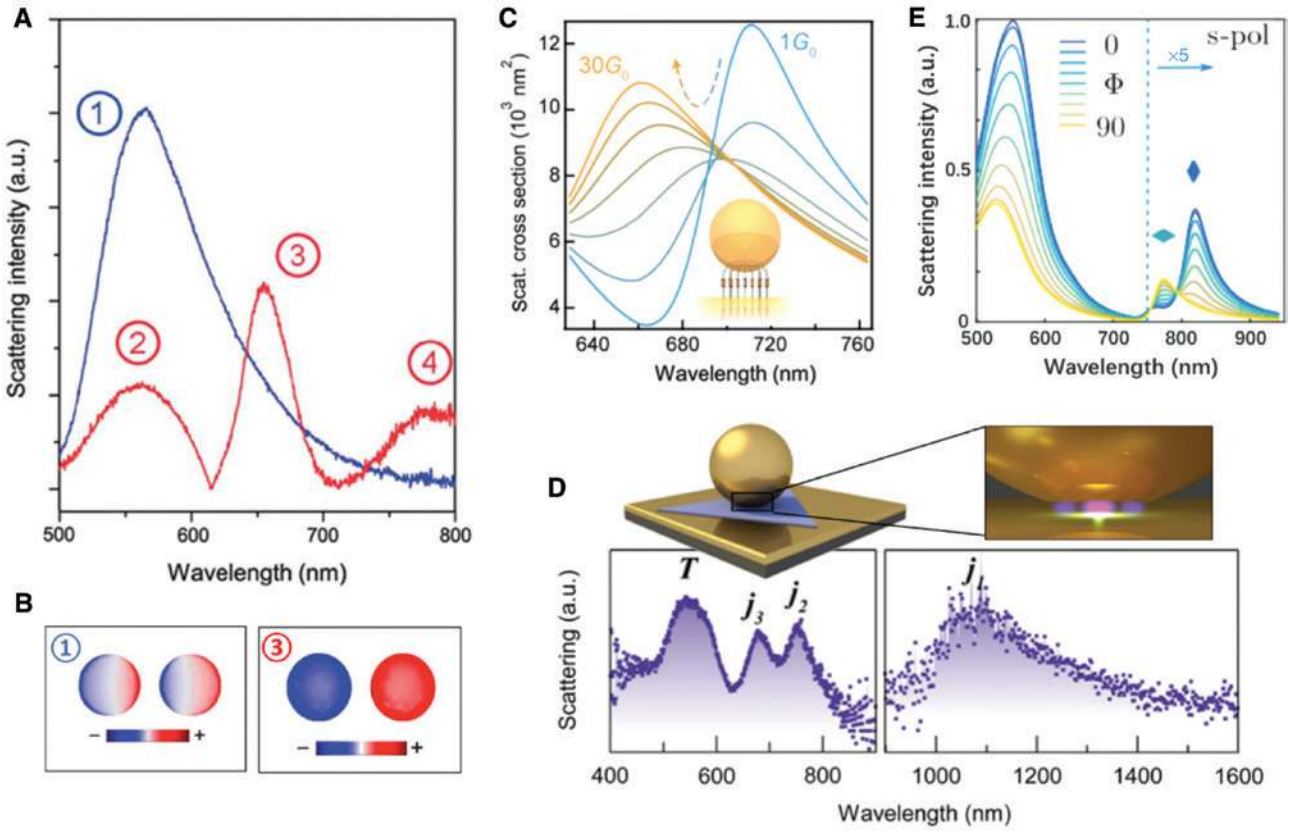

Figure 10: Influences of gap contents and morphologies on the gap plasmons.
(A) A gold nanodisk dimer electrically connected *via* the underlying metal film produces CTP mode (labeled as ③ in red curve). The blue curve corresponds to scattering measurement of its counterpart deposited on silica substrate. (B) Simulated charge distributions for the modes indicated in (A), which clearly resolve a CTP mode for the dimer with a conductive bridge formed in the underlying metal film while a dipolar bonding mode for the one with an insulating gap when placed on a dielectric substrate. Extracted from [101]. (C) The conductivities of the gap contents have a large impact on the gap plasmon resonances. The inset shows the artistic illustration for the plasmon modulation mechanism with gap conductivities. Redrawn from [103]. (D) Faceted gold nanospheres coupling to metal film produce transverse cavity modes that are intrinsically dark but can be hybridized with the radiative gap antenna modes for monitoring the gap morphology changes from the far field. Redrawn from [67]. (E) The polarization responses of the cavity modes help to reveal the geometry asymmetry of the particle-film nanocavities. The linear polarization orientations are continuously rotated in the substrate plane. Extracted from [65].

resonance enabling Raman spectroscopy enhancement (Figure 11D–E). Due to their magnetic response, these gapped nanoresonators hold great potentials as building blocks for novel metamaterials [115]. For example, the colloidal nanocubes self-assembled on metal surface can form an optical equivalent of grounded patch antenna [116]. The induced magnetic currents in single patch provide a phase offset over the electric currents. Properly tailoring the resonance properties can make complete canceling between the respective currents and thus efficiently suppress the wave outcoupling (Figure 11B). Since this phase manipulation is insensitive to the interparticle interaction, closely spaced such colloidal nanoparticles randomly assembled on metal film can create a large scale yet highly efficient metasurface absorber within the visible-near-infrared range [111, 117].

More complex plasmonic particle-on-film nanocavities can be created by placing bonded plasmonic nanoparticles (nanoparticle dimers, trimers, etc.) atop metals. While these plasmonic structures can provide rich plasmon resonances [46], the coexistence of particle-particle and particle-film plasmon couplings largely complicates the understanding of their plasmonic responses in an intuitive way. However, a semi-analytical approach is available for the simplest case where a metal nanoparticle dimer is coupled to a metal film. Resorting to simulation results, it has been revealed that, when the incident light is polarized along the dimer axis, the plasmonic responses of the individual film-coupled nanoparticle dimers are determined by the plasmon coupling between the particle-particle bonding dipole and the induced dipole charges in metal film [118]. As illustrated in Figure

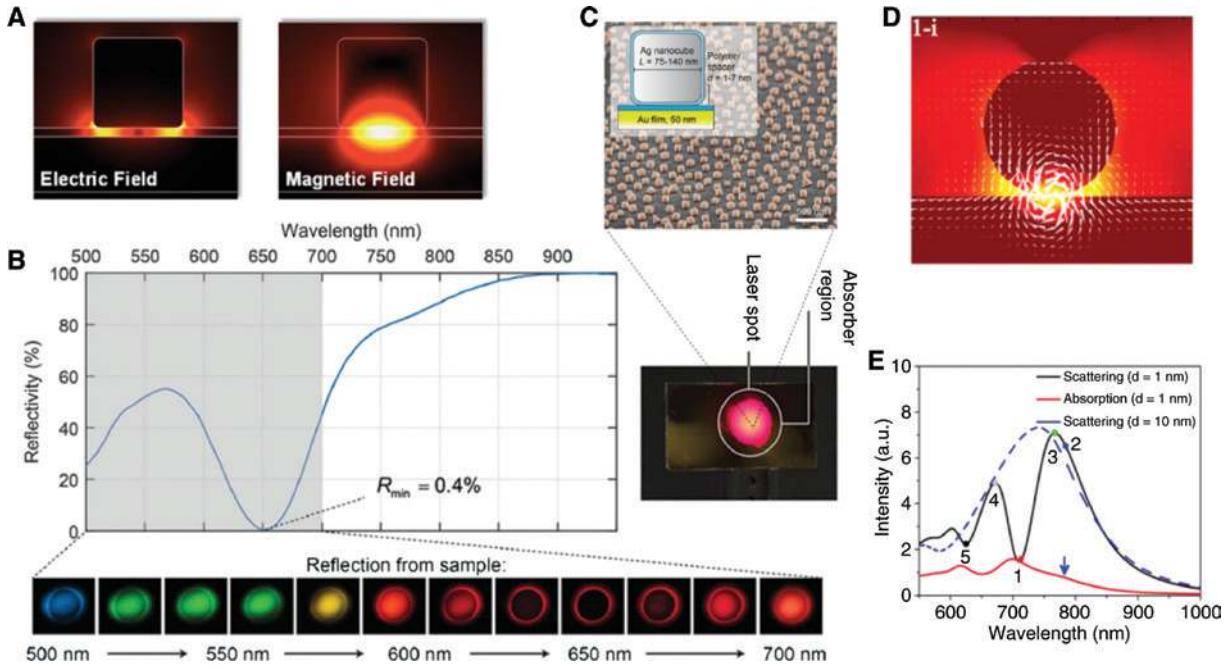

Figure 11: Magnetic responses of the metal film-coupled nanostructures.
(A) Electric and magnetic field intensity distributions of the film-coupled nanocubes at the resonance wavelength as manifested by the spectral dip in (B). Strong confinement of magnetic field occurs inside the gap region. Extracted from [19]. (B) The reflectivity measured for the metasurface formed by high-density nanocubes self-assembled on the metal film. The right image presents the sample illuminated by a laser spot with a diameter slightly larger than the sample area. The bottom sub-images present the sample appearance under illumination of different wavelength laser beams. The red ring-shaped patterns suggest strong light absorption at the illumination wavelengths.
(C) False-color rendered SEM image of the metasurface. The inset illustrates the structure of individual patch antenna as the metasurface elements. Extracted from [111]. (D) The electric displacement vector indicating the formation of a magnetic dipole in the particle-film junction.
(E) Scattering and absorption of large nanoparticles coupled to a metal film. The broad nanoparticle resonance destructively interferences with the gap-mediated magnetic resonance, resulting in the Fano resonance manifested by the dip in scattering spectrum. Extracted from [112].

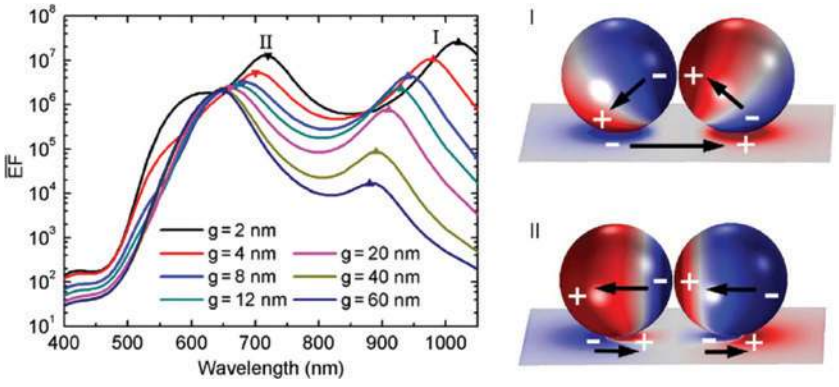

Figure 12: Plasmonic responses of a gold nanoparticle dimer on a thin gold film when the incident plane wave is polarized along the dimer axis.
The left panel shows the numerically calculated averaged near-field enhancement factor spectra for different particle-particle gap distances denoted as "g," while the diameter of the nanoparticles and the particle-film gap distance are fixed at 120 nm and 2 nm, respectively. Two prominent plasmon resonances, labeled as I and II, respectively, are resolved in the near-field enhancement factor spectra. Resonance I originates from the vertical bonding between the dimer dipole and the induced charge dipoles, while the horizontal bonding is responsible for the emerging of resonance II, as confirmed by their corresponding surface charge distributions given in the right panel. Redraw from [118].

12, the vertical and horizontal bonding between the real dimer dipoles and their images in the metal film predicts two prominent resonances, well consisting with the experimental observations in [32, 62]. When the incident light is polarized along the substrate-norm direction, only the particle-film plasmon couplings can be activated. In

the scattering, the film-coupled dimer shows a resonance peak similar to that of a film-coupled monomer, but with nearly doubled radiation intensity (refer to Figures 8 and 16D). This mode actually corresponds to the antibonding of the two vertical particle-image dipole in single film-coupled monomers [62].

We have noticed that the dielectric nanostructures with high refractive index have received increasing research interest in recent years [120]. These structures support rich electric and magnetic multipole Mie-type resonances and can also be placed atop metals to modify their mode responses. The research topics associated with these dielectric-metal hybrid nanostructures have been addressed in a number of studies; the interested reader may refer to [121–124].

In the subsequent sections, we will review the advanced applications benefitting from the plasmonic nanocavities formed by metal nanoparticle-on-film structures, which includes several topics covering the SERS spectroscopy, spontaneous emission, photocatalysis, and molecular nanochemistry. Each section begins with a brief introduction of the topic background, followed by a detailed discussion and review, which demonstrate the unique advantages or opportunities of MPoFNs offered for such spectroscopy applications and extreme physical effects.

5 Raman spectroscopy and cavity optomechanics

Raman spectroscopy is the method used to study inelastic light scattering in matters, usually molecular systems. The frequency shift of the scattered light with respect to the incident photon produces the Stokes or anti-Stokes scattering components (Figure 13A), which can provide detailed chemical and structural information on the material systems. However, the Raman scattering cross-sections of common active molecules are found to be intrinsically small (typically 10^{10} times smaller than the absorption cross section of fluorescence) [127], resulting in a rather low detection efficiency, limiting their practical applications. Since the first demonstration of plasmon-assisted Raman spectroscopy [128], SERS has received intensive investigation during the past two decades. It has now been well established that the SERS observed at rough metal surface or in plasmonic nanostructures dominantly

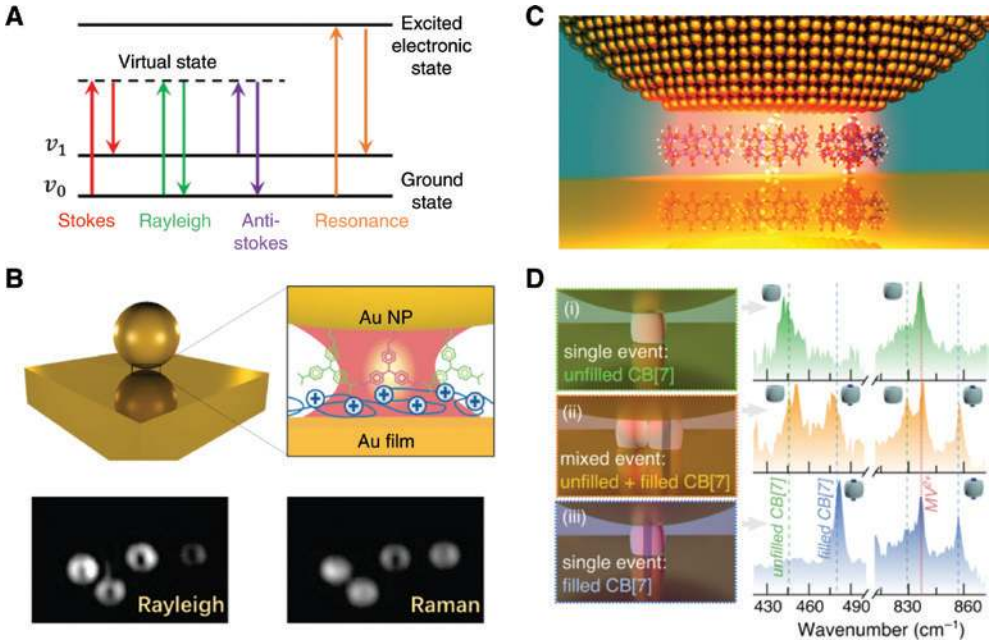

Figure 13: Molecular Raman spectroscopy enhancement by metal particle-film nanocavities.
(A) Energy diagram illustrating the Raman processes, including the stokes, anti-stokes, and resonance enhanced Raman. Redrawn from [63]. (B) Raman scattering enhancement by the strong field localization in the metal particle-film nanocavities. Bottom images show the Rayleigh (left) and Raman (right) scattering patterns of individual plasmonic nanocavities coupled with malachite green isothiocyanate (MGITC). Extracted from [125]. (C–D) Artistical view of the plasmonic nanogaps hosting Cucurbit[7]uril filled with Raman active molecules. The distinct Raman features resolved for the different gap contents and their configuration demonstrate the ability to monitor molecular dynamics at the nanoscale. Extracted from [126].

originates from the strong field localization due to LSPs as well as the chemical enhancement due to induced charge transfer between metals and molecules, although with negligible contributions. Thus, SERS research in the near past has been oriented to practical applications, particularly toward the development of highly efficient SERS substrates for biochemical sensing with single-molecule sensitivity and advanced Raman spectroscopy tools enabling nanoscale chemical imaging.

The nanogaps formed by metal nanoparticles on film enable extremely strong localization and field enhancement of incident electromagnetic waves, thus acting as excellent plasmonic substrates for large SERS enhancement [125, 129]. Although the absorption dipole moments of self-assembled Raman molecules within the particle-film nanogaps preferentially lie in the substrate plane, significant Raman scattering signal can be detected when the gap plasmon resonances are spectrally tuned to match the molecule absorption resonance and roughly the excitation wavelength (Figure 13B). The radiation patterns of such SERS signal from single nanoparticles on film exhibit doughnut-shaped profiles, similar to that of Rayleigh scattering at the wavelength of gap plasmon resonance, suggesting that a small number of molecules roughly aligned along the local plasmonic fields contribute to the total Raman signals. When the absorption dipoles of the Raman molecules are optimally aligned with the particle-film nanocavity, the Raman signals from single molecules can even been captured (Figure 13C–D). This extraordinarily enhanced SERS efficiency by MPoFNs thus renders them excellent SERS probes to explore the local plasmonic fields [93, 130] and monitor the molecular and chemical dynamics at the nanoscale [126, 131].

Conventional Raman scattering from bulk materials is size independent. But distinct Raman responses can be predicted when the bulks are shrunk to the nanoscale. This has been extensively demonstrated with the layered 2D semiconductor materials, which exhibit layer-dependent Raman features [132]. However, the dominant Raman responses originate from the in-plane-polarized modes. A recent study using MPoFNs successfully resolved the out-of-plane Raman modes of nanometer-thick semiconductor platelets [133], which is confirmed impossible with the excitation configuration in conventional Raman spectroscopy setup or accessible only with complex near-field probe technologies such as tip-enhanced Raman scattering [134]. It has been revealed that the dominant longitudinal field components within the nanogap selectively excite the out-of-plane vibrational modes, while the usually bright in-plane modes are largely suppressed due to weaker in-plane field components (Figure 14)

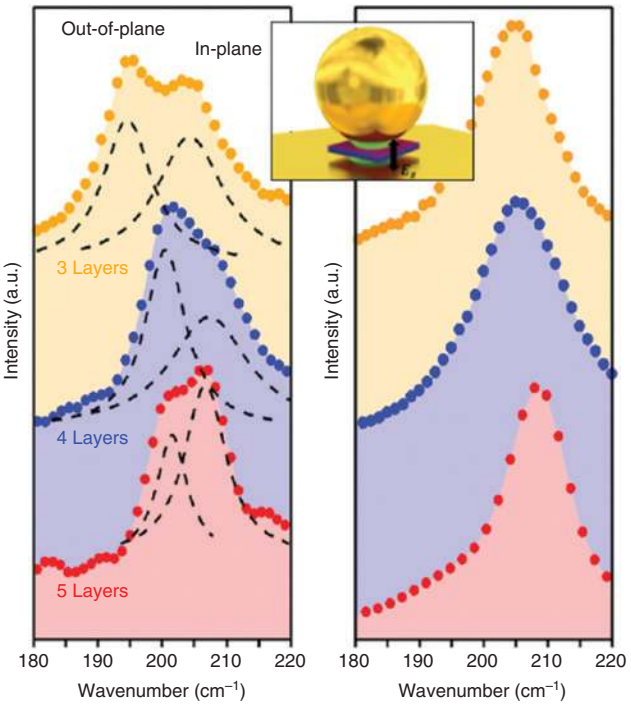

Figure 14: Out-of-plane Raman and excitonic emissions exclusively enhanced by the dominant out-of-plane gap plasmonic fields within the metal nanocavities.
The out-of-plane phonon modes of the nanometer-thick semiconductor platelets are successfully resolved by sandwiching them in the particle-film nanogaps (left), while their cavity-free counterpart shows only the in-plane modes, which exhibit thickness-independent responses. The inset shows the schematic construct of the nanostructures in the studies. Redrawn from [133].

distributed near the gap junctions. Likewise, the same strategy is also adopted to resolve the out-of-plane emission of dark excitons in 2D materials, using a similar plasmonic nanocavity formed by a metal tip hanging above the metal film, but with significantly reduced collection efficiency of optical signals [135].

Importantly, the ultracompact MPoFN offers a promising platform to study the molecular cavity optomechanics that focuses on the interaction between light and molecular vibrations inside cavities [136]. Pulsed Raman scattering of molecules embedded in metal particle-film nanogap reveals superlinear Stokes emission above a threshold (Figure 15C–D), suggesting a reversible optomechanical driving that is the precursor of molecular parametric instability (equivalent to a phonon laser or "phaser" regime) [137]. It has also been found that the induced cavity and molecular changes at a high pump rate can terminate this phonon amplification process. Nevertheless, the laser-activated mobilization of surface atoms in the gap junction can be significantly suppressed

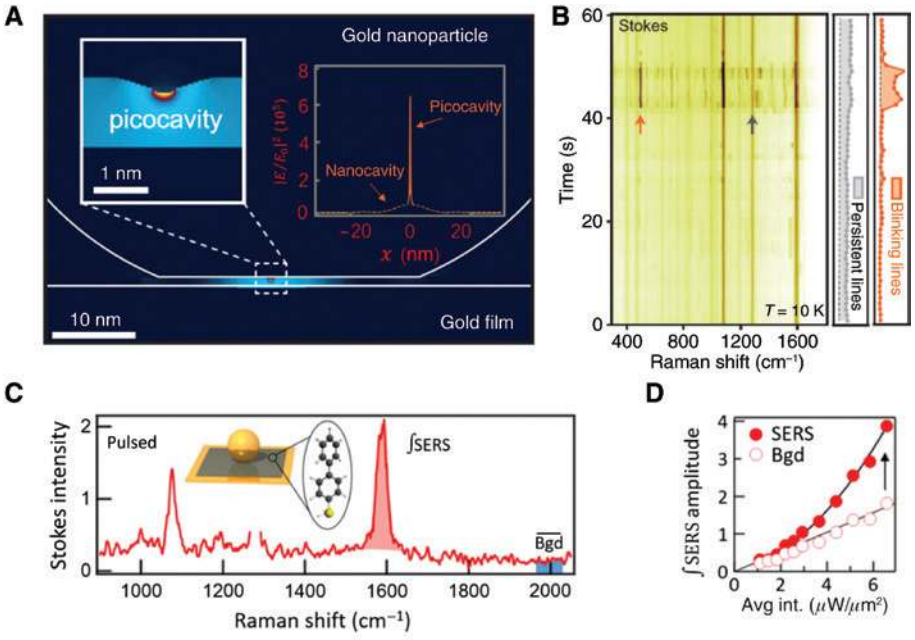

Figure 15: Study of cavity optomechanics using metal film-coupled nanoparticles.
(A) Near-field intensity distribution in the gold particle-film nanocavity. Within this nanocavity, a gold protrusion with atomic size forms a picocavity, which results in cascaded ultrastrong plasmonic confinement. Insets show the enlarged near-field intensity distribution within the nanogap to highlight the picocavity (left) and the picocavity enabled cascaded field enhancement (right). Redrawn from [28].
(B) Low-temperature time-series SERS spectra of monolayer biphenyl-4-thoil (BPT) incorporated into the single gold particle-film nanocavity. The observed vibration modes can be divided into two sets: the first set is ever-present with constant intensity, and the other set is with blinking appearance, which suggests a single molecule event. Extracted from [28]. (C–D) Stokes SERS spectra of BPT molecules inside the gold particle-film nanocavities with excitation by pulsed lasers and pump power dependences of the emission intensity of the SERS signals and their background. Inset in (C) shows the schematic of the hybrid structure of BPT monolayer sandwiched inside the particle-film nanocavity. Extracted from [137].

at cryogenic temperatures. This allows the formation of a stable atomic-sized metal protrusion, functioned as a picocavity (Figure 15A–B), to be probed for many minutes [28]. The ultrastrong light localization by these picocavities not only alters the number and variety of vibrational modes of trapped molecules but also enables optomechanics enhancement at the single-molecule level.

6 Spontaneous emission and photoluminescence enhancement

Spontaneous emission corresponds to the process in which a quantum emitter system (such as an atom, a molecule, or a quantum dot [QD]) transits from an excited energy state to a lower energy state (e.g. ground state) and relaxes the energy difference *via* emitting a photon. This emission mechanism underlies most of light phenomena such as fluorescence, luminescence, phosphorescence, etc. According to Fermi's golden rule, the spontaneous emission rate not only depends on the intrinsic properties of the emitter itself but also can be modified by the extrinsic electromagnetic environments. In general, the spontaneous decay rate of a dipolar emitter is given by

$$\gamma_{sp}(\vec{r}) = \frac{\pi\omega}{3\hbar\varepsilon_0}\left|p\right|^2 \rho(\vec{r},\omega) + \gamma_{int}^0, \quad (1)$$

where ω is the emission frequency, p is the dipole moment of the emitter, $\vec{r}$ represents the position, ε_0 is the free space permittivity, and γ_{int}^0 is the nonradiative decay rate of the emitter. The local density of optical states (LDOS) $\rho(\vec{r},\omega)$ is written as

$$\rho(\vec{r},\omega) \propto n_p \cdot \mathrm{Im}\{G(\vec{r},\vec{r})\} \cdot n_p, \quad (2)$$

where n_p is the orientation of the transition dipole and $G(\vec{r},\vec{r})$ is the dyadic Green's function, which describes the electric field interaction with the emitter due to its own radiation.

Considering the influence of the LDOS on the decay rate, early approaches concentrate on integrating emitters into dielectric micro-resonators to achieve spontaneous emission enhancement. The acceleration of spontaneous

decay rate with resonators, known as Purcell effect, can be expressed as the ratio of the decay rate of the emitter in the resonator to that in the vacuum environment. In dielectric resonators, the Purcell factor can be formulated as $F_P \sim \frac{Q}{V}$, in which the quality factor Q represents the photon confinement with respect to time, whereas the mode volume V represents it with respect to space [138]. Achieving large Purcell factors requires the dielectric resonators to possess large Q factors or/and small mode volumes. Dielectric cavities can have relatively large Q factors at cryogenic temperature but are typically <100 at room temperature. In addition, their mode volumes can hardly reach the sub-wavelength scale for further confinement of light. In addition, to optimize the cavity-emitter coupling, significant fabrication effort is required to spectrally tune the narrowband cavity mode to match the emitter emission. Plasmonic cavity structures often suffer significant metal dissipation and radiation loss and thus are featured with relatively small Q factors (typically below 100). However, their broad resonance linewidth can largely facilitate the spectral matching between the cavity modes and the resonance of embedded emitters. In plasmonic cavities, the Purcell factor is corrected as $F_P \sim Re\left(\frac{Q}{V}\right) \sim \frac{1}{V^2}$ [139]. Due to the strong field confinement of LSPs, the corresponding cavity mode volumes can readily be shrunk to the deep-subwavelength even sub-nanometer scale. MPoFNs are especially attractive plasmonic platforms for obtaining large spontaneous emission enhancement, not only because they support cavity plasmonic modes with ultra-small mode volumes but also because of their flexibly tunable resonance positions and ease of integrating emitters into the particle-film nanocavities.

A large variety of emitters can be fed into MPoFNs, such as fluorescent molecules [140], QDs [141], nitrogen-vacancy centers [142], and monolayered 2D semiconductor materials [143]. By sandwiching a thin dye molecule layer in between a silver nanowire and film (Figure 16A), Kasey J. Russell and coworkers reported radiative spontaneous emission rate enhancement approaching three orders of magnitude with respect to that of the cavity-free

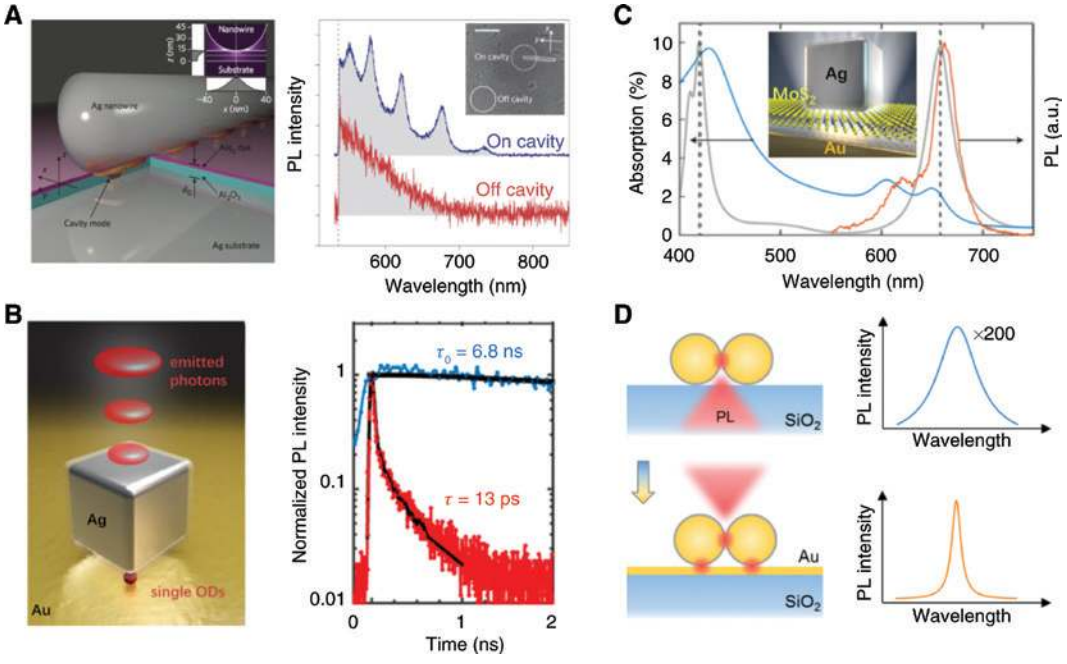

Figure 16: Spontaneous emission enhancement of plasmonic nanocavity coupled emitters.
(A) Large Purcell enhancement obtained for molecular emitters embedded in the metal nanowire-film nanocavity. Left inset: near-field intensity distribution of the nanoconstruct. Right inset: SEM image of the sample area of interest. Extracted from [25]. (B) Single semiconductor QDs coupled to the patch nanoantenna enables an ultrafast emission rate, creating an efficient yet bright single photon source. The blue curve represents the emission decay for single QDs on glass, while the red one, for nanocavity-coupled single QDs. Extracted from [119]. (C) Two-dimensional semiconductor materials sandwiched in the nanoparticle-film nanocavity largely enhance their light absorption and photon yield simultaneously. The gray curve corresponds to the scattering response of the nanocavity structure. Redrawn from [31]. (D) Enhanced spontaneous emission of the gold nanoparticle dimers on film. The pronounced emission linewidth shrinking of the dimer on gold film with respect to its counterpart on glass suggests an emission process through radiative plasmon decay. Extracted from [32].

emitters [25]. Despite the close proximity of metal surfaces, the emitters positioned in the nanocavity exhibit high internal quantum efficiency. Gap size control experiments and calculations revealed that the strengthened coupling between the molecule emission and plasmon cavity modes at reduced gap distance is responsible for the enhanced emission intensity. While the spontaneous decay can be decomposed into the radiative and nonradiative channel, it has been revealed that the radiative decay dominantly contributes to the total decay rate. Replacing the nanowire with a plasmonic nanoantenna, such as nanocubes (Figure 16B), the plasmon-assisted emission enhancement can be further improved through the optical antenna effect [26]. With spectral matching between the cavity antenna mode and the emission of the emitter, a quantum efficiency as high as >0.5 can be obtained, while simultaneously maintaining highly directional emission. By varying the size of the nanoantenna, the cavity plasmon resonances can be tuned across a wide spectral band, encompassing the excitation, absorption, and emission of the emitters, and thus renders a strategy to control the radiative spontaneous emission process *via* plasmons [140, 144]. Semiconductor QDs stand for a promising spontaneous emission source because of their size-dependent emission wavelength, high quantum efficiency at room temperature, and excellent photostability [145]. Integrating QDs into the particle-film nanocavity has demonstrated not only significantly enhanced spontaneous emission intensity but also ultrafast (<11 ps) emission rate [146]. Particularly, the size of semiconductor QDs is typically on the 1–10 nm scale. This largely relaxes the difficulty in positioning single photon emitters into the sizable particle-film nanocavity, thus providing an excellent candidate for creating efficient and bright single photon sources at room temperature [119, 142]. The special geometry of MPoFNs is particularly attractive for the newly emerging semiconductor 2D materials. The monolayered semiconductor materials, belonging to a direct band type, are fluorescent and natural candidates for being as the loading emitters [147]. The semiconductor 2D materials are typically featured by low light absorption and emission efficiency [148], but enhanced light-matter interactions can be achieved by integrating them into plasmonic nanostructures [149–152]. As discussed in Section 4, the film-coupled nanostructures usually support multiple plasmon resonances due to the strong near-field interaction between the plasmonic elements. These tunable multiple resonances make it possible to spectrally match one of them with the absorption peak of the fluorescent 2D materials, while another one with its emission peak. Such spectral mode-matching configuration, together with spatial overlapping between the matched modes (Figure 16C), permits a significant absorption enhancement for the cavity-coupled emitters at the excitation wavelength and, simultaneously, a large photon yield at the emission wavelength [31, 144].

For the emitter-free nanoparticle-film cavities, even the intrinsically weak spontaneous emission of the metal itself can be strongly enhanced by the ultrastrong mode confinement [153]. Intense emission has been observed in single gold film-coupled nanoparticles dimer [32]. While this nanoconstruct is featured by multiple gap nanocavities, i.e. the particle-particle and particle-film gaps, calculation results reveal that the metal atoms near the particle-film gaps dominantly contribute to the total emission enhancement. The measured emission shares similar spectral characters with their scattering, unambiguously confirming the nature of the emission process through radiative plasmon decay (Figure 16D). Nevertheless, the mechanism for light emission from plasmonic metals remains controversial [153–156]. For excitation photon energies below direct interband transitions, the recent study with metal nanoparticles-on-film constructs confirms that light emission by plasmonic metals cannot be ascribed to the common "luminescence " due to intraband transitions but governed by the prompt electronic Raman scattering (ERS), which does not require carrier relaxation [157]. Compared to MPoFNs composed of Au, significant emission improvement was observed with Ag, consisting with the prediction by ERS model. It has to be pointed out that in these MPoFNs with ultrasmall nanogaps, the emission quenching effect is not as pronounced as in the common case that an emitter closely approaches bare metal surfaces [158]. Instead, the emission quenching effect is significantly suppressed, largely due to the increased radiation efficiency of high-order modes through which the emission decays [159, 160].

While the spontaneous emission enhancement with resonators addressed here is restricted to MPoFNs, a number of comprehensive reviews describing the spontaneous emission process in a wide spectrum of resonant structures, including both the conventional dielectric microcavities and metal-based plasmonic nanocavities, can be found in the appended references [161, 162].

7 Photocatalysis and nanochemistry

MPoFNs also demonstrated their vast potential in photocatalysis and nanochemistry applications. Past studies

confirmed that the strong field localization can significantly prompt the production of electron-hole pairs in the nanogap-hosted cadmium selenide (CdSe) nanoplatelets (Figure 17A), which largely facilitates hydrogen production using solar-powered water splitting [163]. Upon resonant excitation, an Au/TiO_2-dumbbell-on-film nanocavity serves

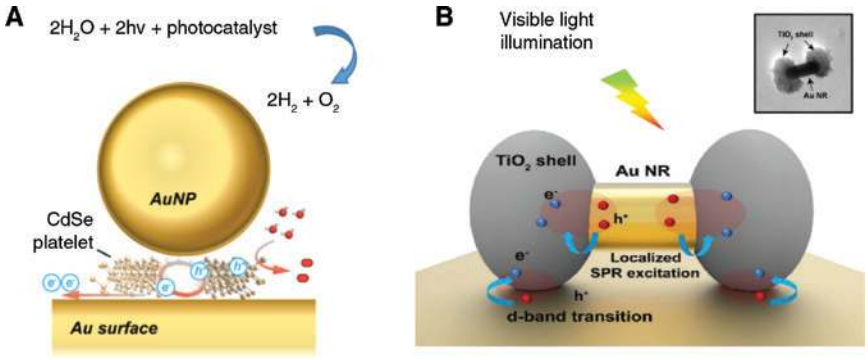

Figure 17: Metal particle-film nanocavities increasing the efficiency of photocatalytic water splitting.
(A) The extremely strong field intensity within the nanocavity increases the electron-hole pair production in the ultrathin CdSe platelet and enhances the interfacial electron transfer for water splitting. Redrawn from [163]. (B) For the Au/TiO_2 dumbbell nanostructures assembled on the Au film, upon resonant excitation of the gap plasmons, the energetic electrons produced in Au can be injected over the Au/TiO_2 Schottky barrier and migrate to TiO_2, accelerating the chemical reaction occurring at the TiO_2 surface. The inset shows the transmission electron microscopy micrograph of the Au/TiO_2 nanostructures. Extracted from [164].

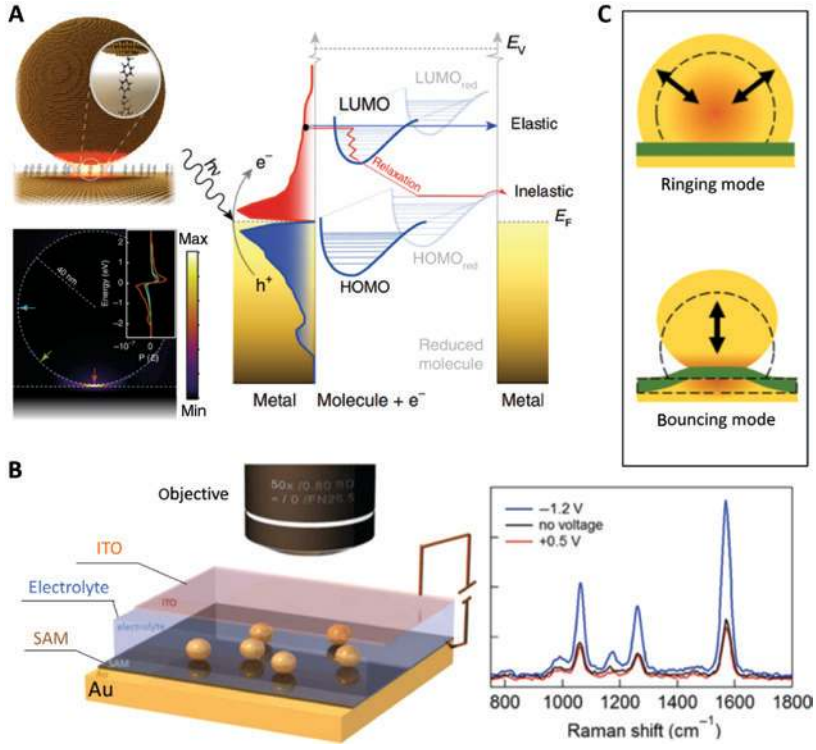

Figure 18: Metal particle-film nanocavities for nanochemistry applications.
(A) The plasmonic fields in the nanoparticle-on-film establish an initial hot carrier population following the near-field distribution (lower-left, inset shows the carrier population). Such distribution allows for the coherent tunneling of electrons between the facing metals. As illustrated in the right column, this tunneling can transit to the hopping type when embedding molecules that increase the tunneling barriers, rendering the observation of single-molecule redox chemistry. Extracted from [165]. (B) Experimental setup for tracking single-nanoparticle-based nanoelectrochemistry (left) and measured SERS spectra under different biases. Extracted from [166]. (C) The large field localization in the metal particle-film nanogap enables ultrastrong coupling between the gap plasmons and the acoustic modes, which can help to measure the contact area of individual nanoparticles. Extracted from [167].

as an efficient light absorber and hot-carrier generator in the visible region, resulting in remarkable enhancement of both the photocurrent production and chemical reaction rate at the TiO_2 surface (Figure 17B) [164].

In the electrochemistry experiments in Figure 18B, applying a negative bias over the particle-film gap junction leads to enhanced Raman signals for all vibrational modes of the cavity-hosted molecules [166]. This has been confirmed to be caused by the H^+ reduction from the solvent electrolyte environments. Such ion transport further results in competition between the nanoparticle charging and the electron tunneling through the gapped molecule layer, which establishes nonequilibrium currents to shift electrons along the molecule layers and change the SERS intensity. These effects demonstrate that the isolated metal particle-film nanogap junction can be exploited to track the dynamics of nanoscale electrochemistry, possible even at the single molecule level (Figure 18A) [165].

The metal nanocavities formed by nanoparticle-film constructs are believed to benefit probing other physical effects and processes, such as plasmonic coupling to mechanical vibrations enabling the characterization of acoustic resonances *via* gap plasmons (Figure 18C) [167]. Too many research and application aspects remain to be explored with this advanced plasmonic platform, but our review and discussions will end here.

8 Conclusion and outlook

In this overview article, we comprehensively reviewed many aspects of MPoFNs, including the fabrication techniques of constructing such nanostructures with atomically smooth surface and controllable gap distance ranging from a few angstroms to tens of nanometers, the typical optical setups and configurations to characterize their plasmon responses, discussions with great details on their rich plasmon modes and promising applications in SERS spectroscopy, spontaneous emission, as well as the vast potential in photocatalysis and nanochemistry.

It has to been pointed out that while most of the studies reviewed here involve the plasmonic nanocavities formed by single nanoparticles coupled to film, the studies about complex nanostructures (dimers, trimers, etc.) coupled to films remain relatively scarce [32, 118]. Such advanced structures with multiple particle-particle and particle-film plasmon couplings are expected to offer richer resonances and more freedoms to tailor their optical properties. In addition, precise placement of single dipole emitters into the plasmonic nanocavity for optimal coupling has always been a challenge but is highly required for achieving spontaneous emission enhancement and light-mater interaction in the strong coupling regime. Although the single-molecule strong coupling has been demonstrated with such gold particle-film nanocavity, the loading of the single molecule into this nanocavity in an optimal configuration still remains an occasional event [27]. More reliable approaches need to be developed to fulfill the advantages offered by MPoFNs.

Acknowledgments: This work was supported by the National Natural Science Foundation of China (Funder Id: http://dx.doi.org/10.13039/501100001809, Grant No. 11474240) and The Hong Kong Polytechnic University (Grant Nos. G-YBPV and 1-ZVGH).

References

[1] Jaque D, Martinez Maestro L, del Rosal B, et al. Nanoparticles for photothermal therapies. Nanoscale 2014;6:9494–530.
[2] Hutter E, Maysinger D. Gold nanoparticles and quantum dots for bioimaging. Microsc Res Tech 2011;74:592–604.
[3] Schlucker S. SERS microscopy: nanoparticle probes and biomedical applications. Chemphyschem 2009;10:1344–54.
[4] Mohamed MB, Volkov V, Link S, El-Sayed MA. The "lightning" gold nanorods: fluorescence enhancement of over a million compared to the gold metal. Chem Phys Lett 2000;317:517–23.
[5] Zhang S, Li GC, Chen Y, et al. Pronounced Fano resonance in single gold split nanodisks with 15 nm split gaps for intensive second harmonic generation. ACS Nano 2016;10:11105–14.
[6] Liu SD, Leong ES, Li GC, et al. Polarization-independent multiple Fano resonances in plasmonic nonamers for multimode-matching enhanced multiband second-harmonic generation. ACS Nano 2016;10:1442–53.
[7] Tsai CY, Lin JW, Wu CY, Lin PT, Lu TW, Lee PT. Plasmonic coupling in gold nanoring dimers: observation of coupled bonding mode. Nano Lett 2012;12:1648–54.
[8] Sonnefraud Y, Verellen N, Sobhani H, et al. Experimental realization of subradiant, superradiant, and fano resonances in ring/disk plasmonic nanocavities. ACS Nano 2010;4:1664–70.
[9] Luk'yanchuk B, Zheludev NI, Maier SA, et al. The Fano Resonance in plasmonic nanostructures and metamaterials. Nat Mater 2010;9:707–15.
[10] Englund D, Faraon A, Fushman I, Stoltz N, Petroff P, Vuckovic J. Controlling cavity reflectivity with a single quantum dot. Nature 2007;450:857–61.
[11] Nomura M, Kumagai N, Iwamoto S, Ota Y, Arakawa Y. Laser oscillation in a strongly coupled single-quantum-dot-nanocavity system. Nat Phys 2010;6:279–83.
[12] Mock JJ, Hill RT, Degiron A, Zauscher S, Chilkoti A, Smith DR. Distance-dependent plasmon resonant coupling between a gold nanoparticle and gold film. Nano Lett 2008;8:2245–52.
[13] Lumdee C, Yun B, Kik PG. Effect of surface roughness on substrate-tuned gold nanoparticle gap plasmon resonances. Nanoscale 2015;7:4250–5.

[14] Mubeen S, Zhang S, Kim N, et al. Plasmonic properties of gold nanoparticles separated from a gold mirror by an ultrathin oxide. Nano Lett 2012;12:2088–94.
[15] Yu B, Woo J, Kong M, O'Carroll DM. Mode-specific study of nanoparticle-mediated optical interactions in an absorber/metal thin film system. Nanoscale 2015;7:13196–206.
[16] Schertz F, Schmelzeisen M, Mohammadi R, Kreiter M, Elmers HJ, Schonhense G. Near field of strongly coupled plasmons: uncovering dark modes. Nano Lett 2012;12:1885–90.
[17] Mock JJ, Hill RT, Tsai YJ, Chilkoti A, Smith DR. Probing dynamically tunable localized surface plasmon resonances of film-coupled nanoparticles by evanescent wave excitation. Nano Lett 2012;12:1757–64.
[18] Ha JW, Marchuk K, Fang N. Focused orientation and position imaging (FOPI) of single anisotropic plasmonic nanoparticles by total internal reflection scattering microscopy. Nano Lett 2012;12:4282–8.
[19] Lassiter JB, McGuire F, Mock JJ, et al. Plasmonic waveguide modes of film-coupled metallic nanocubes. Nano Lett 2013;13:5866–72.
[20] Lei DY, Fernandez-Dominguez AI, Sonnefraud Y, et al. Revealing plasmonic gap modes in particle-on-film systems using dark-field spectroscopy. ACS Nano 2012;6:1380–6.
[21] Hill RT, Mock JJ, Hucknall A, et al. Plasmon ruler with Angstrom length resolution. ACS Nano 2012;6:9237–46.
[22] Ciraci C, Hill RT, Mock JJ, et al. Probing the ultimate limits of plasmonic enhancement. Science 2012;337:1072–4.
[23] Hajisalem G, Nezami MS, Gordon R. Probing the quantum tunneling limit of plasmonic enhancement by third harmonic generation. Nano Lett 2014;14:6651–4.
[24] Oulton RF, Sorger VJ, Zentgraf T, et al. Plasmon lasers at deep subwavelength scale. Nature 2009;461:629–32.
[25] Russell KJ, Liu TL, Cui SY, Hu EL. Large spontaneous emission enhancement in plasmonic nanocavities. Nat Photonics 2012;6:459–62.
[26] Akselrod GM, Argyropoulos C, Hoang TB, et al. Probing the mechanisms of large Purcell enhancement in plasmonic nanoantennas. Nat Photonics 2014;8:835–40.
[27] Chikkaraddy R, de Nijs B, Benz F, et al. Single-molecule strong coupling at room temperature in plasmonic nanocavities. Nature 2016;535:127–30.
[28] Benz F, Schmidt MK, Dreismann A, et al. Single-molecule optomechanics in "picocavities". Science 2016;354:726–9.
[29] Itoh T, Yamamoto YS, Ozaki Y. Plasmon-enhanced spectroscopy of absorption and spontaneous emissions explained using cavity quantum optics. Chem Soc Rev 2017;46:3904–21.
[30] George SM. Atomic layer deposition: an overview. Chem Rev 2010;110:111–31.
[31] Akselrod GM, Ming T, Argyropoulos C, et al. Leveraging nanocavity harmonics for control of optical processes in 2D semiconductors. Nano Lett 2015;15:3578–84.
[32] Li GC, Zhang YL, Jiang J, Luo Y, Lei DY. Metal-substrate-mediated plasmon hybridization in a nanoparticle dimer for photoluminescence line-width shrinking and intensity enhancement. ACS Nano 2017;11:3067–80.
[33] Decher G. Fuzzy Nanoassemblies: toward layered polymeric multicomposites. Science 1997;277:1232–7.
[34] Lumdee C, Yun BF, Kik PG. Wide-band spectral control of Au nanoparticle plasmon resonances on a thermally and chemically robust sensing platform. J Phys Chem C 2013;117:19127–33.
[35] Esteban R, Zugarramurdi A, Zhang P, et al. A classical treatment of optical tunneling in plasmonic gaps: extending the quantum corrected model to practical situations. Faraday Discuss 2015;178:151–83.
[36] Zhu W, Crozier KB. Quantum mechanical limit to plasmonic enhancement as observed by surface-enhanced Raman scattering. Nat Commun 2014;5:5228.
[37] Mortensen NA, Raza S, Wubs M, Sondergaard T, Bozhevolnyi SI. A generalized non-local optical response theory for plasmonic nanostructures. Nat Commun 2014;5:3809.
[38] Mertens J, Eiden AL, Sigle DO, et al. Controlling subnanometer gaps in plasmonic dimers using graphene. Nano Lett 2013;13:5033–8.
[39] Kleemann ME, Chikkaraddy R, Alexeev EM, et al. Strong-coupling of Wse2 in ultra-compact plasmonic nanocavities at room temperature. Nat Commun 2017;8:1296.
[40] Manzeli S, Ovchinnikov D, Pasquier D, Yazyev OV, Kis A. 2D transition metal dichalcogenides. Nat Rev Mater 2017;2:17033.
[41] Zhang Y, Zhang L, Zhou C. Review of chemical vapor deposition of graphene and related applications. Acc Chem Res 2013;46:2329–39.
[42] Yu X, Lei DY, Amin F, et al. Distance control in-between plasmonic nanoparticles via biological and polymeric spacers. Nano Today 2013;8:480–93.
[43] Yang L, Wang H, Fang Y, Li Z. Polarization state of light scattered from quantum plasmonic dimer antennas. ACS Nano 2016;10:1580–8.
[44] Shen S, Meng L, Zhang Y, et al. Plasmon-enhanced second-harmonic generation nanorulers with ultrahigh sensitivities. Nano Lett 2015;15:6716–21.
[45] Wang X, Li M, Meng L, et al. Probing the location of hot spots by surface-enhanced Raman spectroscopy: toward uniform substrates. ACS Nano 2014;8:528–36.
[46] Chen S, Meng LY, Shan HY, et al. How to light special hot spots in multiparticle-film configurations. ACS Nano 2016;10:581–7.
[47] Ding T, Sigle D, Zhang L, Mertens J, de Nijs B, Baumberg J. Controllable tuning plasmonic coupling with nanoscale oxidation. ACS Nano 2015;9:6110–8.
[48] Ding T, Mertens J, Lombardi A, Scherman OA, Baumberg JJ. Light-directed tuning of plasmon resonances via plasmon-induced polymerization using hot electrons. ACS Photonics 2017;4:1453–8.
[49] Lumdee C, Toroghi S, Kik PG. Post-fabrication voltage controlled resonance tuning of nanoscale plasmonic antennas. ACS Nano 2012;6:6301–7.
[50] Smith DL. Thin-film deposition: principles and practice, 1st ed. New York, NY: McGraw-Hill Education, 1995.
[51] Zhao Y, Liu X, Lei DY, Chai Y. Effects of surface roughness of Ag thin films on surface-enhanced Raman spectroscopy of graphene: spatial nonlocality and physisorption strain. Nanoscale 2014;6:1311–7.
[52] Butt HJ, Wang DN, Hansma PK, Kühlbrandt W. Effect of surface roughness of carbon support films on high-resolution electron diffraction of two-dimensional protein crystals. Ultramicroscopy 1991;36:307–18.
[53] Butt HJ, Muller T, Gross H. Immobilizing biomolecules for scanning force microscopy by embedding in carbon. J Struct Biol 1993;110:127–32.

[54] Hegner M, Wagner P, Semenza G. Ultralarge atomically flat template-stripped au surfaces for scanning probe microscopy. Surf Sci 1993;291:39–46.
[55] Rueda A, Vogel N, Kreiter M. Characterization of gold films by surface plasmon spectroscopy: large errors and small consequences. Surf Sci 2009;603:491–7.
[56] Weiss EA, Kaufman GK, Kriebel JK, Li Z, Schalek R, Whitesides GM. Si/Sio2-templated formation of ultraflat metal surfaces on glass, polymer, and solder supports: their use as substrates for self-assembled monolayers. Langmuir 2007;23:9686–94.
[57] Vogel N, Zieleniecki J, Koper I. As flat as it gets: ultrasmooth surfaces from template-stripping procedures. Nanoscale 2012;4:3820–32.
[58] Sau TK, Murphy CJ. Room temperature, high-yield synthesis of multiple shapes of gold nanoparticles in aqueous solution. J Am Chem Soc 2004;126:8648–9.
[59] Guo ZR, Zhang Y, DuanMu Y, Xu L, Xie SL, Gu N. Facile synthesis of micrometer-sized gold nanoplates through an aniline-assisted route in ethylene glycol solution. Colloid Surface A 2006;278:33–8.
[60] Huang JS, Callegari V, Geisler P, et al. Atomically flat single-crystalline gold nanostructures for plasmonic nanocircuitry. Nat Commun 2010;1:150.
[61] Panaro S, Nazir A, Liberale C, et al. Dark to bright mode conversion on dipolar nanoantennas: a symmetry-breaking approach. ACS Photonics 2014;1:310–4.
[62] Li GC, Zhang YL, Lei DY. Hybrid plasmonic gap modes in metal film-coupled dimers and their physical origins revealed by polarization resolved dark field spectroscopy. Nanoscale 2016;8:7119–26.
[63] Zrimsek AB, Chiang N, Mattei M, et al. Single-molecule chemistry with surface- and tip-enhanced Raman spectroscopy. Chem Rev 2017;117:7583–613.
[64] Panoiu NC, Sha WEI, Lei DY, Li GC. Nonlinear optics in plasmonic nanostructures. J Optics-UK 2018;20:083001.
[65] Kleemann ME, Mertens J, Zheng X, et al. Revealing nanostructures through plasmon polarimetry. ACS Nano 2017;11:850–5.
[66] Li AR, Isaacs S, Abdulhalim I, Li SZ. Ultrahigh enhancement of electromagnetic fields by exciting localized with extended surface plasmons. J Phys Chem C 2015;119:19382–9.
[67] Sigle DO, Mertens J, Herrmann LO, et al. Monitoring morphological changes in 2D monolayer semiconductors using atom-thick plasmonic nanocavities. ACS Nano 2015;9:825–30.
[68] Chikkaraddy R, Zheng XZ, Benz F, et al. How ultranarrow gap symmetries control plasmonic nanocavity modes: from cubes to spheres in the nanoparticle-on-mirror. ACS Photonics 2017;4:469–75.
[69] Ciraci C, Lassiter JB, Moreau A, Smith DR. Quasi-analytic study of scattering from optical plasmonic patch antennas. J Appl Phys 2013;114:163108.
[70] Bautista G, Kauranen M. Vector-field nonlinear microscopy of nanostructures. ACS Photonics 2016;3:1351–70.
[71] Kozawa Y, Sato S. Observation of the longitudinal field of a focused laser beam by second-harmonic generation. J Opt Soc Am B 2008;25:175–9.
[72] Bauer T, Orlov S, Peschel U, Banzer P, Leuchs G. Nanointerferometric amplitude and phase reconstruction of tightly focused vector beams. Nat Photonics 2014;8:24–8.
[73] Novotny L, Beversluis MR, Youngworth KS, Brown TG. Longitudinal field modes probed by single molecules. Phys Rev Lett 2001;86:5251–4.
[74] Bautista G, Makitalo J, Chen Y, et al. Second-harmonic generation imaging of semiconductor nanowires with focused vector beams. Nano Lett 2015;15:1564–9.
[75] Long J, Yi H, Li H, Lei Z, Yang T. Reproducible ultrahigh SERS enhancement in single deterministic hotspots using nanosphere-plane antennas under radially polarized excitation. Sci Rep 2016;6:33218.
[76] You S, Kuang C, Toussaint KC, Jr., Zhou R, Xia X, Liu X. Iterative phase-retrieval method for generating stereo array of polarization-controlled focal spots. Opt Lett 2015;40:3532–5.
[77] Liu SC, You ST, Fang Y, Wang YF, Kuang CF, Liu X. Effects of polarization and phase modulation on the focal spot in 4pi microscopy. J Mod Optic 2016;63:1145–57.
[78] Huang CZ, Wu MJ, Chen SY. High order gap modes of film-coupled nanospheres. J Phys Chem C 2015;119:13799–806.
[79] Trivedi R, Thomas A, Dhawan A. Full-wave electromagentic analysis of a plasmonic nanoparticle separated from a plasmonic film by a thin spacer layer. Opt Express 2014;22:19970–89.
[80] Benz F, de Nijs B, Tserkezis C, et al. Generalized circuit model for coupled plasmonic systems. Opt Express 2015;23:33255–69.
[81] Yang JJ, Hugonin JP, Lalanne P. Near-to-far field transformations for radiative and guided waves. ACS Photonics 2016;3:395–402.
[82] Prodan E, Radloff C, Halas NJ, Nordlander P. A hybridization model for the plasmon response of complex nanostructures. Science 2003;302:419–22.
[83] Willingham B, Brandl DW, Nordlander P. Plasmon hybridization in nanorod dimers. Appl Phys B-Lasers O 2008;93:209–16.
[84] Wu Y, Nordlander P. Plasmon hybridization in nanoshells with a nonconcentric core. J Chem Phys 2006;125:124708.
[85] Wang H, Wu Y, Lassiter B, et al. Symmetry breaking in individual plasmonic nanoparticles. Proc Natl Acad Sci U S A 2006;103:10856–60.
[86] Nordlander P, Prodan E. Plasmon hybridization in nanoparticles near metallic surfaces. Nano Lett 2004;4:2209–13.
[87] Pendry JB, Aubry A, Smith DR, Maier SA. Transformation optics and subwavelength control of light. Science 2012;337:549–52.
[88] Pendry JB, Luo Y, Zhao RK. Transforming the optical landscape. Science 2015;348:521–4.
[89] Pacheco-Peña V, Beruete M, Fernández-Domínguez AI, Luo Y, Navarro-Cía M. Description of bow-tie nanoantennas excited by localized emitters using conformal transformation. ACS Photonics 2016;3:1223–32.
[90] Pendry JB, Fernandez-Dominguez AI, Luo Y, Zhao RK. Capturing photons with transformation optics. Nat Phys 2013;9:518–22.
[91] Lei DY, Aubry A, Luo Y, Maier SA, Pendry JB. Plasmonic interaction between overlapping nanowires. ACS Nano 2011;5:597–607.
[92] Lei DY, Aubry A, Maier SA, Pendry JB. Broadband nano-focusing of light using kissing nanowires. New J Phys 2010;12:093030.
[93] Lombardi A, Demetriadou A, Weller L, et al. Anomalous spectral shift of near- and far-field plasmonic resonances in nanogaps. ACS Photonics 2016;3:471–7.
[94] Aubry A, Lei DY, Maier SA, Pendry JB. Plasmonic hybridization between nanowires and a metallic surface: a transformation optics approach. ACS Nano 2011;5:3293–308.

[95] Leveque G, Martin OJ. Tunable composite nanoparticle for plasmonics. Opt Lett 2006;31:2750–2.
[96] Wu YP, Nordlander P. Finite-Difference time-domain modeling of the optical properties of nanoparticles near dielectric substrates. J Phys Chem C 2010;114:7302–7.
[97] Driskell JD, Lipert RJ, Porter MD. Labeled gold nanoparticles immobilized at smooth metallic substrates: systematic investigation of surface plasmon resonance and surface-enhanced Raman scattering. J Phys Chem B 2006;110:17444–51.
[98] Zhu W, Esteban R, Borisov AG, et al. Quantum mechanical effects in plasmonic structures with subnanometre gaps. Nat Commun 2016;7:11495.
[99] Sobhani A, Manjavacas A, Cao Y, et al. Pronounced linewidth narrowing of an aluminum nanoparticle plasmon resonance by interaction with an aluminum metallic film. Nano Lett 2015;15:6946–51.
[100] Rueda A, Stemmler M, Bauer R, Mullen K, Fogel Y, Kreiter M. Optical resonances of gold nanoparticles on a gold surface: quantitative correlation of geometry and resonance wavelength. New J Phys 2008;10:113001.
[101] Wang Y, Li Z, Zhao K, et al. Substrate-mediated charge transfer plasmons in simple and complex nanoparticle clusters. Nanoscale 2013;5:9897–901.
[102] Liu H, Ng J, Wang SB, Hang ZH, Chan CT, Zhu SN. Strong plasmon coupling between two gold nanospheres on a gold slab. New J Phys 2011;13:073040.
[103] Benz F, Tserkezis C, Herrmann LO, et al. Nanooptics of molecular-shunted plasmonic nanojunctions. Nano Lett 2015;15:669–74.
[104] Wilson WM, Stewart JW, Mikkelsen MH. Surpassing single line width active tuning with photochromic molecules coupled to plasmonic nanoantennas. Nano Lett 2018;18:853–8.
[105] Chen XX, Yang YQ, Chen YH, Qiu M, Blaikie RJ, Ding BY. Probing plasmonic gap resonances between gold nanorods and a metallic surface. J Phys Chem C 2015;119:18627–34.
[106] Sugimoto H, Yashima S, Fujii M. Hybridized plasmonic gap mode of gold nanorod on mirror nanoantenna for spectrally tailored fluorescence enhancement. ACS Photonics 2018;5:3421–7.
[107] Tserkezis C, Esteban R, Sigle DO, et al. Hybridization of plasmonic antenna and cavity modes: extreme optics of nanoparticle-on-mirror nanogaps. Phys Rev A 2015;92:053811.
[108] Filter R, Qi J, Rockstuhl C, Lederer F. Circular optical nanoantennas: an analytical theory. Phys Rev B 2012;85:125429.
[109] Esteban R, Teperik TV, Greffet JJ. Optical patch antennas for single photon emission using surface plasmon resonances. Phys Rev Lett 2010;104:026802.
[110] Mertens J, Demetriadou A, Bowman RW, et al. Tracking Optical welding through groove modes in plasmonic nanocavities. Nano Lett 2016;16:5605–11.
[111] Akselrod GM, Huang J, Hoang TB, et al. Large-area metasurface perfect absorbers from visible to near-infrared. Adv Mater 2015;27:8028–34.
[112] Chen S, Zhang Y, Shih TM, et al. Plasmon-induced magnetic resonance enhanced Raman spectroscopy. Nano Lett 2018;18:2209–16.
[113] Chen JD, Xiang J, Jiang S, Dai QF, Tie SL, Lan S. Radiation of the high-order plasmonic modes of large gold nanospheres excited by surface plasmon polaritons. Nanoscale 2018;10:9153–63.
[114] Liu Y, Palomba S, Park Y, Zentgraf T, Yin X, Zhang X. Compact magnetic antennas for directional excitation of surface plasmons. Nano Lett 2012;12:4853–8.
[115] Klein MW, Enkrich C, Wegener M, Linden S. Second-harmonic generation from magnetic metamaterials. Science 2006;313:502–4.
[116] Moreau A, Ciraci C, Mock JJ, et al. Controlled-reflectance surfaces with film-coupled colloidal nanoantennas. Nature 2012;492:86–9.
[117] Huang FM, Drakeley S, Millyard MG, et al. Zero-reflectance metafilms for optimal plasmonic sensing. Adv Opt Mater 2016;4:328–35.
[118] Huang Y, Ma L, Hou M, Li J, Xie Z, Zhang Z. Hybridized plasmon modes and near-field enhancement of metallic nanoparticle-dimer on a mirror. Sci Rep 2016;6:30011.
[119] Hoang TB, Akselrod GM, Mikkelsen MH. Ultrafast room-temperature single photon emission from quantum dots coupled to plasmonic nanocavities. Nano Lett 2016;16:270–5.
[120] Krasnok A, Caldarola M, Bonod N, Alu A. Spectroscopy and biosensing with optically resonant dielectric nanostructures. Adv Opt Mater 2018;6:1701094.
[121] Li H, Xu Y, Xiang J, et al. Exploiting the interaction between a semiconductor nanosphere and a thin metal film for nanoscale plasmonic devices. Nanoscale 2016;8:18963–71.
[122] Sinev I, Iorsh I, Bogdanov A, et al. Polarization control over electric and magnetic dipole resonances of dielectric nanoparticles on metallic films. Laser Photonics Rev 2016;10:799–806.
[123] Kuo YL, Chuang SY, Chen SY, Chen KP. Enhancing the interaction between high-refractive index nanoparticles and gold film substrates based on oblique incidence excitation. ACS Omega 2016;1:613–9.
[124] Sugimoto H, Fujii M. Broadband dielectric-metal hybrid nanoantenna: silicon nanoparticle on a mirror. ACS Photonics 2018;5:1986–93.
[125] Hill RT, Mock JJ, Urzhumov Y, et al. Leveraging nanoscale plasmonic modes to achieve reproducible enhancement of light. Nano Lett 2010;10:4150–4.
[126] Sigle DO, Kasera S, Herrmann LO, et al. Observing single molecules complexing with cucurbit[7]uril through nanogap surface-enhanced Raman spectroscopy. J Phys Chem Lett 2016;7:704–10.
[127] Kneipp K, Moskovits M, Kneipp H. Surface-enhanced Raman scattering. Berlin Heidelberg: Springer-Verlag, 2006.
[128] Fleischmann M, Hendra PJ, Mcquillan AJ. Raman-spectra of pyridine adsorbed at a silver electrode. Chem Phys Lett 1974;26:163–6.
[129] Chen SY, Mock JJ, Hill RT, Chilkoti A, Smith DR, Lazarides AA. Gold nanoparticles on polarizable surfaces as Raman scattering antennas. ACS Nano 2010;4:6535–46.
[130] Du L, Lei DY, Yuan G, et al. Mapping plasmonic near-field profiles and interferences by surface-enhanced Raman scattering. Sci Rep 2013;3:3064.
[131] Di Martino G, Tappertzhofen S, Hofmann S, Baumberg J. Nanoscale plasmon-enhanced spectroscopy in memristive switches. Small 2016;12:1334–41.
[132] Zhang X, Qiao XF, Shi W, Wu JB, Jiang DS, Tan PH. Phonon and Raman scattering of two-dimensional transition metal dichalcogenides from monolayer, multilayer to bulk material. Chem Soc Rev 2015;44:2757–85.

[133] Sigle DO, Hugall JT, Ithurria S, Dubertret B, Baumberg JJ. Probing confined phonon modes in individual CDSE nanoplatelets using surface-enhanced Raman scattering. Phys Rev Lett 2014;113:087402.
[134] Schmid T, Opilik L, Blum C, Zenobi R. Nanoscale chemical imaging using tip-enhanced Raman spectroscopy: a critical review. Angew Chem Int Ed Engl 2013;52:5940–54.
[135] Park KD, Jiang T, Clark G, Xu X, Raschke MB. Radiative control of dark excitons at room temperature by nano-optical antenna-tip Purcell effect. Nat Nanotechnol 2018;13:59–64.
[136] Roelli P, Galland C, Piro N, Kippenberg TJ. Molecular cavity optomechanics as a theory of plasmon-enhanced Raman scattering. Nat Nanotechnol 2016;11:164–9.
[137] Lombardi A, Schmidt MK, Weller L, et al. Pulsed molecular optomechanics in plasmonic nanocavities: from nonlinear vibrational instabilities to bond-breaking. Phys Rev X 2018;8:011016.
[138] Purcell EM. Spontaneous emission probabilities at radio frequencies. Physical Review 1946;69:681.
[139] Sauvan C, Hugonin JP, Maksymov IS, Lalanne P. Theory of the spontaneous optical emission of nanosize photonic and plasmon resonators. Phys Rev Lett 2013;110:237401.
[140] Rose A, Hoang TB, McGuire F, et al. Control of radiative processes using tunable plasmonic nanopatch antennas. Nano Lett 2014;14:4797–802.
[141] Yashima S, Sugimoto H, Takashina H, Fujii M. Fluorescence enhancement and spectral shaping of silicon quantum dot monolayer by plasmonic gap resonances. J Phys Chem C 2016;120:28795–801.
[142] Bogdanov SI, Shalaginov MY, Lagutchev AS, et al. Ultrabright room-temperature sub-nanosecond emission from single nitrogen-vacancy centers coupled to nanopatch antennas. Nano Lett 2018;18:4837–44.
[143] Cheng F, Johnson AD, Tsai Y, et al. Enhanced photoluminescence of monolayer Ws2 on Ag Films and nanowire-Ws2-Film Composites. ACS Photonics 2017;4:1421–30.
[144] Huang J, Akselrod GM, Ming T, Kong J, Mikkelsen MH. Tailored emission spectrum of 2D Semiconductors using plasmonic nanocavities. ACS Photonics 2018;5:552–8.
[145] Kim JY, Voznyy O, Zhitomirsky D, Sargent EH. 25th Anniversary article: colloidal quantum dot materials and devices: a quarter-century of advances. Adv Mater 2013;25:4986–5010.
[146] Hoang TB, Akselrod GM, Argyropoulos C, Huang J, Smith DR, Mikkelsen MH. Ultrafast spontaneous emission source using plasmonic nanoantennas. Nat Commun 2015;6:7788.
[147] Wu ZQ, Yang JL, Manjunath NK, et al. Gap-mode surface-plasmon-enhanced photoluminescence and photoresponse of Mos2. Adv Mater 2018;30:e1706527.
[148] Mak KF, He K, Lee C, et al. Tightly bound trions in monolayer Mos2. Nat Mater 2013;12:207–11.
[149] Wen J, Wang H, Wang W, et al. Room-temperature strong light-matter interaction with active control in single plasmonic nanorod coupled with two-dimensional atomic crystals. Nano Lett 2017;17:4689–97.
[150] Zheng D, Zhang S, Deng Q, Kang M, Nordlander P, Xu H. Manipulating coherent plasmon-exciton interaction in a single silver nanorod on monolayer Wse2. Nano Lett 2017;17:3809–14.
[151] Cuadra J, Baranov DG, Wersäll M, Verre R, Antosiewicz TJ, Shegai T. Observation of tunable charged exciton polaritons in hybrid monolayer Ws2-plasmonic nanoantenna system. Nano Lett 2018;18:1777–85.
[152] Wen J, Wang H, Chen H, Deng S, Xu N. Room-temperature strong coupling between dipolar plasmon resonance in single gold nanorod and two-dimensional excitons in monolayer Wse2. Chin Phys B 2018;27:096101.
[153] Lumdee C, Yun BF, Kik PG. Gap-plasmon enhanced gold nanoparticle photoluminescence. ACS Photonics 2014;1:1224–30.
[154] Haug T, Klemm P, Bange S, Lupton JM. Hot-electron intraband luminescence from single hot spots in noble-metal nanoparticle films. Phys Rev Lett 2015;115:067403.
[155] Huang D, Byers CP, Wang LY, et al. Photoluminescence of a Plasmonic Molecule. ACS Nano 2015;9:7072–9.
[156] Fang Y, Chang WS, Willingham B, Swanglap P, Dominguez-Medina S, Link S. Plasmon Emission quantum yield of single gold nanorods as a function of aspect ratio. ACS Nano 2012;6:7177–84.
[157] Mertens J, Kleemann ME, Chikkaraddy R, Narang P, Baumberg JJ. How light is emitted by plasmonic metals. Nano Lett 2017;17:2568–74.
[158] Anger P, Bharadwaj P, Novotny L. Enhancement and quenching of single-molecule fluorescence. Phys Rev Lett 2006;96:113002.
[159] Kongsuwan N, Demetriadou A, Chikkaraddy R, et al. Suppressed quenching and strong-coupling of Purcell-enhanced single-molecule emission in plasmonic nanocavities. ACS Photonics 2018;5:186–91.
[160] Faggiani R, Yang JJ, Lalanne P. Quenching, plasmonic, and radiative decays in nanogap emitting devices. ACS Photonics 2015;2:1739–44.
[161] Pelton M. Modified spontaneous emission in nanophotonic structures. Nat Photonics 2015;9:427–35.
[162] Tsakmakidis KL, Boyd RW, Yablonovitch E, Zhang X. Large spontaneous-emission enhancements in metallic nanostructures: towards LEDs faster than lasers. Opt Express 2016;24:17916–27.
[163] Sigle DO, Zhang L, Ithurria S, Dubertret B, Baumberg JJ. Ultrathin CDSE in Plasmonic nanogaps for enhanced photocatalytic water splitting. J Phys Chem Lett 2015;6:1099–103.
[164] Ho KHW, Shang A, Shi F, et al. Plasmonic Au/Tio2-dumbbell-on-film nanocavities for high-efficiency hot-carrier generation and extraction. Adv Funct Mater 2018;28:1800383.
[165] de Nijs B, Benz F, Barrow SJ, et al. Plasmonic tunnel junctions for single-molecule redox chemistry. Nat Commun 2017;8:994.
[166] Di Martino G, Turek VA, Lombardi A, et al. Tracking nanoelectrochemistry using individual plasmonic nanocavities. Nano Lett 2017;17:4840–5.
[167] Deacon WM, Lombardi A, Benz F, et al. Interrogating nanojunctions using ultraconfined acoustoplasmonic coupling. Phys Rev Lett 2017;119:023901.